Sci. Dril., 32, 1–25, 2023
https://doi.org/10.5194/sd-32-1-2023

Scientific Drilling
Open Access

Initial results of coring at Prees, Cheshire Basin, UK (ICDP JET project): towards an integrated stratigraphy, timescale, and Earth system understanding for the Early Jurassic

Stephen P. Hesselbo[1], Aisha Al-Suwaidi[2], Sarah J. Baker[3], Giorgia Ballabio[4], Claire M. Belcher[3], Andrew Bond[5], Ian Boomer[6], Remco Bos[7], Christian J. Bjerrum[8], Kara Bogus[1], Richard Boyle[3], James V. Browning[9], Alan R. Butcher[10], Daniel J. Condon[11], Philip Copestake[12], Stuart Daines[3], Christopher Dalby[1], Magret Damaschke[11], Susana E. Damborenea[13], Jean-Francois Deconinck[14], Alexander J. Dickson[5], Isabel M. Fendley[15], Calum P. Fox[16], Angela Fraguas[17], Joost Frieling[15], Thomas A. Gibson[1], Tianchen He[18], Kat Hickey[1], Linda A. Hinnov[19], Teuntje P. Hollaar[1,3], Chunju Huang[20], Alexander J. L. Hudson[1], Hugh C. Jenkyns[15], Erdem Idiz[15], Mengjie Jiang[1], Wout Krijgsman[7], Christoph Korte[8], Melanie J. Leng[11], Timothy M. Lenton[3], Katharina Leu[21], Crispin T. S. Little[22], Conall MacNiocaill[15], Miguel O. Manceñido[13], Tamsin A. Mather[15], Emanuela Mattioli[23], Kenneth G. Miller[9], Robert J. Newton[23], Kevin N. Page[1], József Pálfy[24,25], Gregory Pieńkowski[26,†], Richard J. Porter[1], Simon W. Poulton[22], Alberto C. Riccardi[13], James B. Riding[11], Ailsa Roper[22], Micha Ruhl[27], Ricardo L. Silva[28], Marisa S. Storm[29], Guillaume Suan[23], Dominika Szűcs[1], Nicolas Thibault[8], Alfred Uchman[30], James N. Stanley[9], Clemens V. Ullmann[1], Bas van de Schootbrugge[7], Madeleine L. Vickers[31], Sonja Wadas[21], Jessica H. Whiteside[32], Paul B. Wignall[22], Thomas Wonik[21], Weimu Xu[4], Christian Zeeden[21], and Ke Zhao[20]

[1]Camborne School of Mines, Department of Earth and Environmental Sciences, University of Exeter, Penryn Campus, Penryn, Cornwall, TR10 9FE, UK
[2]Department of Earth Sciences, Khalifa University of Science and Technology, P.O. Box 12333, Abu Dhabi, UAE
[3]Department of Geography, Laver Building, University of Exeter, North Park Road, Exeter, EX4 4QE, UK
[4]School of Earth Sciences and SFI Research Centre in Applied Geosciences (iCRAG), University College Dublin, Dublin 4, Ireland
[5]Centre of Climate, Ocean and Atmosphere, Department of Earth Sciences, Royal Holloway University of London, Surrey, TW20 0EX, UK
[6]Geosciences Research Group, School of Geography, Earth and Environmental Sciences, University of Birmingham, Birmingham, B15 2TT, UK
[7]Department of Earth Sciences, Utrecht University, Marine Palynology and Paleoceanography, Princetonlaan 8a, 3584, CB, Utrecht, the Netherlands
[8]Department of Geosciences and Natural Resource Management, University of Copenhagen, Øster Voldgade 10, 1350 Copenhagen-K, Denmark
[9]Department of Earth and Planetary Sciences, Rutgers, the State University of New Jersey, 610 Taylor Road, Piscataway, NJ 08854-8066, USA
[10]Geological Survey of Finland, Espoo, 02151, Finland
[11]British Geological Survey, Keyworth, Nottingham, NG12 5GG, UK
[12]Merlin Energy Resources Ltd., Newberry House, Ledbury, Herefordshire, HR8 2EJ, UK
[13]División Paleozoología Invertebrados, Facultad de Ciencias Naturales y Museo, Universidad Nacional de La Plata, Argentina, CONICET, Paseo del Bosque S/N 1900, La Plata, Argentina
[14]Biogeosciences, UMR 6282, UBFC/CNRS, Université Bourgogne Franche-Comté, 6 Boulevard Gabriel, 21000 Dijon, France

Published by Copernicus Publications on behalf of the IODP and the ICDP.

[15]Department of Earth Sciences, University of Oxford, Oxford, OX1 3AN, UK
[16]Biogeochemistry Center, Japan Agency for Marine-Earth Science and Technology, 2-15 Natsushima-cho Yokosuka 237-0061, Japan
[17]Dpto. Biología y Geología, Física y Química Inorgánica y Grupo de Investigación en Dinámica de la Tierra y Evolución del Paisaje (Dynamical), ESCET, Universidad Rey Juan Carlos, C/Tulipán s/n, 28933 Móstoles, Madrid, Spain
[18]College of Oceanography, Hohai University, 1 Xikang Road, Nanjing, Jiangsu, 210098, China
[19]Department of Atmospheric, Oceanic, and Earth Sciences, George Mason University, Fairfax, VA 22030, USA
[20]State Key Laboratory of Biogeology and Environmental Geology, School of Earth Sciences, China University of Geosciences, Wuhan, China
[21]Leibniz Institute for Applied Geophysics (LIAG), Stilleweg 2, 30655 Hanover, Germany
[22]School of Earth and Environment, University of Leeds, Leeds, LS2 9JT, UK
[23]Univ Lyon, UCBL, ENSL, UJM, CNRS, LGL-TPE, 69622 Villeurbanne, France
[24]Department of Geology, Eötvös Loránd University, Pázmány Péter sétány 1/C, Budapest 1117, Hungary
[25]HUN-REN-MTM-ELTE Research Group of Palaeontology, Pázmány Péter sétány 1/C, Budapest 1117, Hungary
[26]Polish Geological Institute–National Research Institute, Rakowiecka 4, 00-975, Warsaw, Poland
[27]Department of Geology and SFI Research Centre in Applied Geosciences (iCRAG), Trinity College Dublin, The University of Dublin, Dublin, Ireland
[28]Department of Earth Sciences, Clayton H. Riddell Faculty of Earth, Environment, and Resources, University of Manitoba, 230 Wallace Building, 125 Dysart Road, Winnipeg, Manitoba, R3T 2N2, Canada
[29]NIOZ Royal Netherlands Institute for Sea Research, Department of Marine Microbiology and Biogeochemistry, P.O. Box 59, 1790 AB, Den Burg (Texel), the Netherlands
[30]Faculty of Geography and Geology, Jagiellonian University, Gronostajowa 3a, 30-087, Kraków, Poland
[31]Centre for Earth Evolution and Dynamics (CEED), University of Oslo, P.O. Box 1028 Blindern, 0315 Oslo, Norway
[32]Department of Geological Sciences, San Diego State University, San Diego, CA 92182-1010, USA
†deceased, 19 April 2023

Correspondence: Stephen P. Hesselbo (s.p.hesselbo@exeter.ac.uk) and Clemens V. Ullmann (c.ullmann@exeter.ac.uk)

Received: 16 May 2023 – Revised: 30 August 2023 – Accepted: 22 September 2023 – Published: 26 October 2023

Abstract. Drilling for the International Continental Scientific Drilling Program (ICDP) Early Jurassic Earth System and Timescale project (JET) was undertaken between October 2020 and January 2021. The drill site is situated in a small-scale synformal basin of the latest Triassic to Early Jurassic age that formed above the major Permian–Triassic half-graben system of the Cheshire Basin. The borehole is located to recover an expanded and complete succession to complement the legacy core from the Llanbedr (Mochras Farm) borehole drilled through 1967–1969 on the edge of the Cardigan Bay Basin, North Wales. The overall aim of the project is to construct an astronomically calibrated integrated timescale for the Early Jurassic and to provide insights into the operation of the Early Jurassic Earth system. Core of Quaternary age cover and Early Jurassic mudstone was obtained from two shallow partially cored geotechnical holes (Prees 2A to 32.2 m below surface (m b.s.) and Prees 2B to 37.0 m b.s.) together with Early Jurassic and Late Triassic mudstone from the principal hole, Prees 2C, which was cored from 32.92 to 651.32 m (corrected core depth scale). Core recovery was 99.7 % for Prees 2C. The ages of the recovered stratigraphy range from the Late Triassic (probably Rhaetian) to the Early Jurassic, Early Pliensbachian (Ibex Ammonoid Chronozone). All ammonoid chronozones have been identified for the drilled Early Jurassic strata. The full lithological succession comprises the Branscombe Mudstone and Blue Anchor formations of the Mercia Mudstone Group, the Westbury and Lilstock formations of the Penarth Group, and the Redcar Mudstone Formation of the Lias Group. A distinct interval of siltstone is recognized within the Late Sinemurian of the Redcar Mudstone Formation, and the name "Prees Siltstone Member" is proposed. Depositional environments range from playa lake in the Late Triassic to distal offshore marine in the Early Jurassic. Initial datasets compiled from the core include radiography, natural gamma ray, density, magnetic susceptibility, and X-ray fluorescence (XRF). A full suite of downhole logs was also run. Intervals of organic carbon enrichment occur in the Rhaetian (Late Triassic) Westbury Formation and in the earliest Hettangian and

earliest Pliensbachian strata of the Redcar Mudstone Formation, where up to 4 % total organic carbon (TOC) is recorded. Other parts of the succession are generally organic-lean, containing less than 1 % TOC. Carbon-isotope values from bulk organic matter have also been determined, initially at a resolution of ∼ 1 m, and these provide the basis for detailed correlation between the Prees 2 succession and adjacent boreholes and Global Stratotype Section and Point (GSSP) outcrops. Multiple complementary studies are currently underway and preliminary results promise an astronomically calibrated biostratigraphy, magnetostratigraphy, and chemostratigraphy for the combined Prees and Mochras successions as well as insights into the dynamics of background processes and major palaeo-environmental changes.

1 Introduction

1.1 Late Triassic and Early Jurassic Earth and solar system history

The Early Jurassic Earth System and Timescale scientific drilling project (JET) aims to construct a fully integrated and astronomically calibrated timescale for this epoch. This was a time in Earth's history, ∼ 200–175 Ma, when important physical, chemical, and biological elements of the modern Earth system first emerged, for example as expressed in the initial phases of Atlantic Ocean opening (e.g. Torsvik and Cocks, 2017) or the rapid evolution of marine organisms, including planktonic primary carbonate producers (e.g. Knoll and Follows, 2016; Antell and Saupe, 2021; Riding et al., 2023). At the same time, other elements of the Earth system had distinctly Mesozoic characteristics, such as generally warm climate states, the presence of extensive epicontinental seaways susceptible to water mass stratification and anoxia, and short-lived episodes of massive flood basalt volcanism (e.g. Hesselbo et al., 2020a; Remírez and Algeo, 2020; Ruhl et al., 2022).

The interactions between the atmosphere, hydrosphere, biosphere, and lithosphere over Late Triassic to Early Jurassic time have become a focus of much scientific study over the last couple of decades, particularly for the prominent environmental changes that characterize the Triassic–Jurassic transition at ∼ 201 Ma and the Toarcian Oceanic Anoxic Event at ∼ 183 Ma (e.g. Capriolo et al., 2022; Ruhl et al., 2022, and references therein), and much has been learned about the driving processes for mid-Mesozoic climate change, extinction, and evolution. However, the diverse Early Jurassic biostratigraphic, astrochronologic, magnetostratigraphic, and chemostratigraphic schemes have, for the most part, remained poorly integrated with each other and have lacked accurate numerical calibration, leaving many uncertainties with regard to the rates and relative timing of key Earth system processes (e.g. Hesselbo et al., 2020a; Al-Suwaidi et al., 2022). Although astrochronologic studies, which make use of stable orbital cycles, have been used to great advantage recently, incompatible interpretations for the Early Jurassic are not uncommon (see e.g. Ruhl et al., 2016; Weedon et al., 2019; Storm et al., 2020); additionally, because astronomical models cannot accurately constrain orbital histories earlier than the Cenozoic, the pre-Cenozoic rock record is itself crucial for extending knowledge of solar system orbital history into the deep past (Kent et al., 2018; Olsen et al., 2019).

Using a new integrated stratigraphic framework, the JET project aspires to document and quantify the influence of the principal internal and external forcing factors on the Earth system during the Early Jurassic, for both the major palaeo-environmental events and the more stable "background" states between them.

1.2 Site selection, related borehole records, and regional context

The initial focus for this project was on obtaining a new core from the Llanbedr (Mochras Farm) site in the Cardigan Bay Basin (Hesselbo et al., 2013), where previous drilling in the late 1960s had recovered a ∼ 1.3 km thick Mesozoic succession comprising the Rhaetian (Late Triassic), Hettangian, Sinemurian, Pliensbachian, and Toarcian (Early Jurassic) stages, overlain by ∼ 0.6 km of Cenozoic deposits (Wood and Woodland, 1968; Woodland, 1971; Fig. 1). The Early Jurassic mudstone succession at Mochras was found to be biostratigraphically complete at the ammonite zonal level (Woodland, 1971; Dobson and Whittington, 1987; Copestake and Johnson, 2014). The borehole proved to be of great value for understanding UK Jurassic palaeo-geography and basin history, but although the original recovery is calculated as 97.6 % for the Jurassic, only 59.1 % is preserved as core slabs at the British Geological Survey (BGS) National Core Repository, the remainder being either kept as discrete fossil specimens or placed into bags of coarse fragments (∼ 20 mm diameter) representing 5 ft (i.e. ∼ 1.5 m) stratigraphic intervals (Storm et al., 2020). Although much work has been carried out on the legacy Mochras core as part of the JET project (Percival et al., 2016; Ruhl et al., 2016; Baker et al., 2017; Xu et al., 2018a, b; Deconinck et al., 2019; Storm et al., 2020; Hollaar et al., 2021, 2023; Menini et al., 2021; Munier et al., 2021; Pieńkowski et al., 2021; Damaschke et al., 2022; Ruhl et al., 2022; Ullmann et al., 2022; Paulsen and Thibault, 2023), the poor physical state of the lower half of the core (Hettangian and Sinemurian) means any signal of orbital cy-

cles at the fundamental precession scale has been lost, with preserved intact core slabs to a very large degree restricted to the Pliensbachian and Toarcian stages of the cored interval. Similarly, there are no downhole wireline logs for the lower half of the Jurassic succession.

The Mochras site proved to be very challenging on account of its exceptional present-day setting and infrastructural constraints that would have been beyond a practical financial budget to contend with. Because of these considerations at Mochras, a site at Prees, in the neighbouring Cheshire Basin, was selected as an alternative. The Prees site has the principal advantage that the prime stratigraphic targets lie at shallower depths in an environmentally and logistically straightforward location.

The drilled site at Prees represents a similar overall tectonic and depositional setting to Mochras (Penn, 1987; Evans et al., 1993; Tappin et al., 1994; Warrington, 1997; Plant et al., 1999; Fig. 1), Prees being situated within a SW–NE-oriented half-graben called the Wem-Audlem Sub-basin, ∼ 3.2 km NW of the bounding faults of the Wem-Red Rock fault system on its south-eastern margin (Evans et al., 1993; Mikkelsen and Floodpage, 1997).

Two boreholes drilled previously in the Cheshire Basin – "offset wells" – provide a solid stratigraphic background for the Prees location: Wilkesley (Grid Reference SJ 363864 341438), drilled by the British Geological Survey in 1959–1960 to a depth of 1686 m and in its upper part recovering a succession from the Early Jurassic to the Early Triassic, and Prees 1 (Grid Reference SJ 355727 334474), drilled in 1972–1973 by Trend Petroleum for Shell to a depth of 3829 m and penetrating Jurassic to Silurian strata (Fig. 1). Wilkesley was part of an exploration programme that proved salt deposits within the Triassic, and Prees 1 was an exploration well for hydrocarbon resources in possible Triassic and Permian sandstone reservoirs. A shallow borehole at Platt Lane (Grid Reference SJ 351400 336450), drilled for the British Geological Survey in 1959 to 113 m, provides additional core and stratigraphic data around the Triassic–Jurassic boundary. Late Triassic and Jurassic strata were not cored in Prees 1. Although the Hettangian at Wilkesley was fully cored, the core was subsequently broken up, with only hand samples retained at 1 ft (i.e. ∼ 30 cm) intervals together with a series of registered fossil specimens (these latter with significant potential to yield further biostratigraphic, lithological, geochemical, and mineralogical information).

The Hettangian and earliest Sinemurian in the Wilkesley borehole comprise medium- to dark-grey calcareous mudstone with silty mudstone and argillaceous limestone (Poole and Whiteman, 1966). Based on the Prees 1 well completion log together with our examination of cuttings, the entire Early Jurassic succession at Prees was inferred to comprise calcareous mudstone and siltstone with subordinate limestone, a very similar lithological succession to Mochras (Woodland, 1971; Hesselbo et al., 2013; Ruhl et al., 2016; Xu et al., 2018a; Ullmann et al., 2022). Pyrolysis data from Prees 1 cuttings and the Wilkesley core show organic matter maturity to be similar to Mochras, lying on the boundary between immature and mature (Appendix A). Marine calcareous fossils are common in the early Hettangian at Wilkesley, including ammonites, and these have previously allowed a highly resolved ammonite biostratigraphy to be constructed (Donovan in Poole and Whiteman, 1966; Plant et al., 1999). The ammonite succession provides a remarkable record of early recovery faunas after the end-Triassic mass extinction and includes shells with nacreous preservation, i.e. aragonite (Bloos and Page, 2000). A record of foraminifers has also been compiled from the Late Triassic and Early Jurassic of Wilkesley (Copestake, 1989; Copestake and Johnson, 1989).

In total, six exploration wells have been drilled for conventional oil and gas targets in the Cheshire Basin, and all have proven to be dry, likely as a result of the absence of a suitable source rock, particularly in the south of the basin where Prees is located, and due to a lack of closed structures for the early drilled wells (Mikkelsen and Floodpage, 1997; Plant et al., 1999).

2 Methods

2.1 Drilling and logging

Two shallow cored boreholes were drilled for geotechnical characterization of the site between December 2019 and January 2020. These are designated "Prees 2A" (drilled to 32.2 m below surface, m b.s.) and "Prees 2B" (drilled to 37 m b.s.). Drilling and logging operations for the principal borehole, Prees 2C, were carried out from 22 October 2020 to 1 January 2021. Prees 2C reached a total depth (TD) of 651.32 m corrected core depth (m c.c.d.) (see Sect. 2.7 for a description of depth scales for Prees 2C). The primary parameters for the cored boreholes are summarized in Table 1. Full details of the drilling and logging operations are provided in the Operations Report (Hesselbo et al., 2023).

Downhole geophysical data for Prees 2C were acquired by the logging contractor in two runs, from 240 to 33 m depth on 16 November 2020 and for the remainder of the hole after drilling was completed (28 and 29 December 2020). The probes successfully run from ∼ 240 m to the surface were Spectral Gamma Ray, Density, Neutron Porosity, Focused Electric Log, 4-Arm Caliper, Mud Temperature/-Conductivity, Full Wave Sonic, and Acoustic Televiewer. The probes successfully run from TD to 240 m were Spectral Gamma Ray, Density, Neutron Porosity, Induction Log, 4-Arm Caliper, Mud Temperature/Conductivity, Full Wave Sonic, and Acoustic Televiewer.

2.2 Seismic reflection data

The Prees site lies in a region characterized by relatively good seismic coverage including a 1970s vintage low-fold

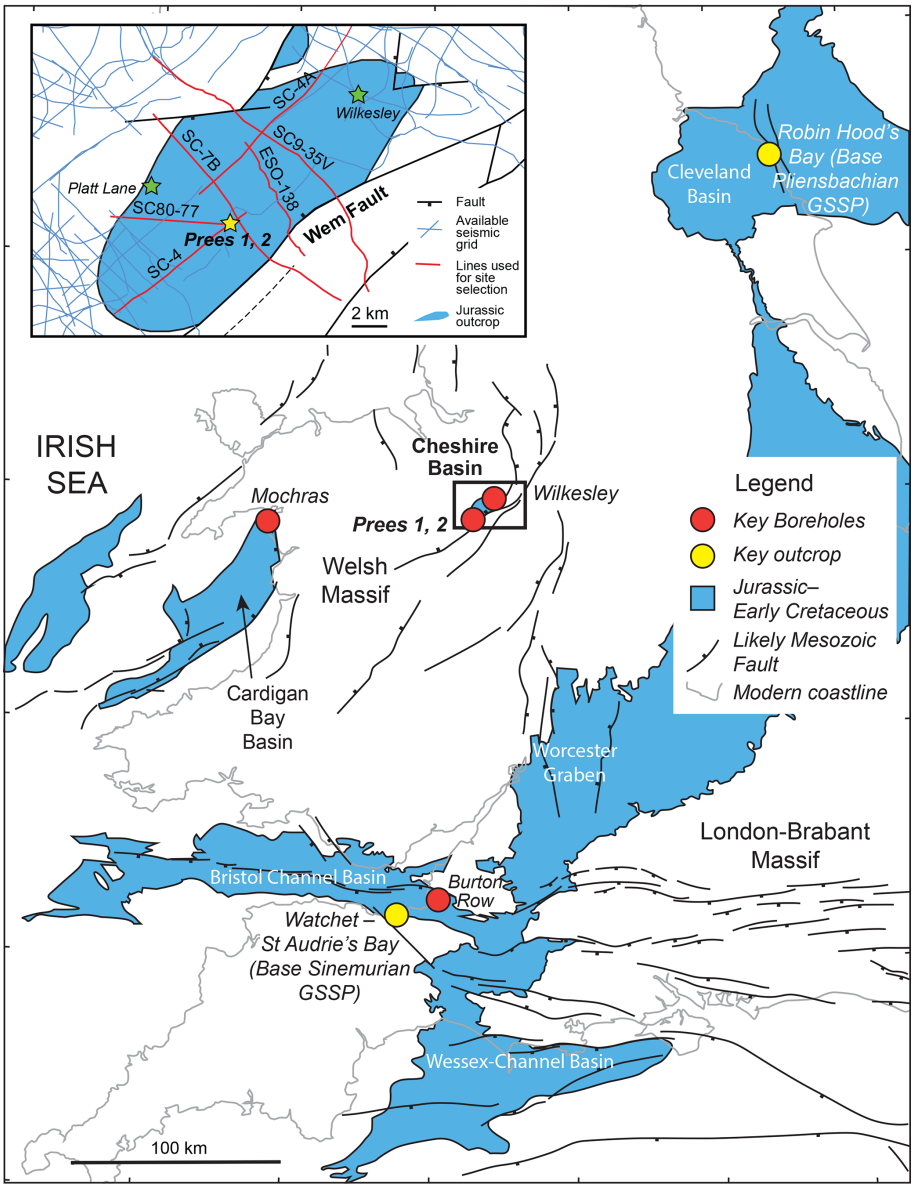

Figure 1. Geological map of Jurassic–Early Cretaceous strata in the southern UK area, showing the locations of the Prees 1 and Prees 2 wells (main map and inset) in relation to the Mochras, Burton Row, Platt Lane, and Wilkesley boreholes as well as outcrop Early Jurassic GSSP sites. The Prees Jurassic outlier (main map and inset) sits in the southern part of the Cheshire Basin. The main figure is based on a BGS 1 : 1 500 000 series tectonic map of the UK, Ireland, and adjacent areas, Sheet 1 (Pharaoh, 1996). The inset is based on data in the UK Onshore Geophysical Library (http://ukogl.org.uk, last access: 6 October 2023). The depositional and tectonic settings of Prees are broadly comparable to Mochras but differ in detail. Green stars in the inset give offset well locations.

Table 1. Principal parameters for Prees 2 boreholes. OS: Ordnance Survey; WGS84: World Geodetic System 1984; OD: Ordnance Datum; SOBI: Single Onshore Borehole Index; m: metres below surface (Prees 2A and 2B); m c.c.d.: metres corrected core depth (Prees 2C). Refer to Sect. 2.7 for a description of the depth scales. Note: n/a – not applicable.

Name	OS grid reference	Latitude (WGS84)	Longitude (WGS84)	Ground level (m, OD)	Rig floor datum (m)	Final depth (m b.s. or m c.c.d.)	SOBI number
Prees 2A	SJ 55569 34483	52.905933	−2.662053	86.63	n/a	32.2	SJ53SE/52
Prees 2B	SJ 55574 34490	52.905996	−2.661980	86.63	n/a	37.0	SJ53SE/51
Prees 2C	SJ 55559 34478	52.905887	−2.662201	86.48	4.58	651.32	SJ53SE/53

dynamite grid and a denser grid of vibroseis acquired in the late 1970s and 1980s (Mikkelsen and Floodpage, 1997). For site selection, the relevant seismic lines (Fig. 1 inset) were obtained and re-processed where possible. Two seismic reflection profiles were used to help determine the optimum drill site location and provide a basinal context, SC-&B and SC4 (Fig. 1). Line SC-7B is oriented NW–SE, passing 0.5 km from Prees 1 (Figs. 1 and 2). Line SC-7B was acquired in 1970 using a dynamite source with a shot point spacing of approximately 60 to 120 m. Vertical geophones with a spacing of about 60 m were used as receivers, and the recording length was 5 s at a sampling rate of 2 ms. In addition to a recording filter of 12 to 96 Hz, the original processing included, for example, true amplitude recovery, static and dynamic corrections, velocity field determination from NMO curves, stacking, and predictive deconvolution.

More modern seismic processing methods were applied to the dataset to improve the imaging quality, especially of the Jurassic formations. Since the raw data of profile SC-7B were not available, only the post-stack data were used. We applied a frequency–wavenumber filter to eliminate disturbing effects of noisy frequencies, which cover the primary reflections. Spectral balancing was then applied to compensate for frequency attenuation, especially at higher frequencies, to obtain a higher-resolution image of the subsurface. Then the data were slightly smoothed with a non-linear smoothing filter to facilitate the interpretation of the horizons. A finite-difference (FD) time migration was applied to correct the positions of dipping reflectors, collapse diffractions, and further increase spatial resolution. Finally, the data were converted from the time domain to the depth domain to allow joint interpretation of the seismic and borehole data.

2.3 Core processing at the drill site

For Prees 2C, the core was obtained at 6 m lengths with a nominal diameter of 97 mm and a hole size of 161.9 mm. A 7 m long plastic liner was used for all core runs. At the drill site the metal core barrel was transported from the rig floor to the core processing area, where the core catcher was removed and any core therein retained in a short section of liner. The core in its liner was then removed from the core barrel onto a series of trestles, where the position of the top of the core was located through the liner and the liner cut at that point. The core was then pushed from the top to the bottom of the liner, and any excess liner was trimmed to fit. Plastic end-caps were then used to mark the top (blue) and bottom (white) of the entire recovered core, which was then marked up into sections 1 m long from the top, with the bottom section generally being less than 1 m in length. In cases where coherent core catcher sections were obtained, these were combined with the bottom section prior to marking up and section cutting.

Each core section was then individually cut with a rock saw and flushed with water whilst still in the liner to remove most drilling fluid from the outer core surfaces and from within fractures (except the first few cores, down to ∼ 83 m b.s., for which this cleaning was carried out in the BGS National Core Repository). Samples of drilling fluid were retained at intervals for later geochemical analysis. Cleaned core sections were then capped using blue and white end-caps and carried into the core description lab. Each core section was given a rudimentary description and a sample chip was taken from the bottom to form the basis of initial analyses for organic carbon isotopes, carbonate and organic carbon content, and elemental abundances at ∼ 1 m resolution, with a total sample set of 625. All drilling, core processing, and sample data were then entered into the mDIS (the International Continental Scientific Drilling Program (ICDP)'s Drilling Information System Goes Mobile). Core sections were boxed on site and stored in a container until they were transported to the National Core Repository in Keyworth at 2- to 3-week intervals.

Core and core section identification follows standard ICDP and BGS protocols. ICDP identification is based on the following format: project code_site number_hole letter_core number_section number (e.g. for the JET project, Hole Prees 2C, Core 10, Sect. 3, the formulation is 5065_1_C_10_3). Each core section was also assigned a BGS core box number in the following manner. As an example, the core box number CB00354103 was assigned for a whole round, with the same number retained for the Archive half derived from this when slabbed (see below).

2.4 Core processing and scanning at the National Core Repository and Core Scanning Facility (multi-sensor core logger, XRF, optical imagery, photography)

Core curation at the BGS National Core Repository was carried out in parallel with drilling, and all whole round sections that were shipped from the drill site were curated with the designation of the future Archive halves. Once whole round-core scanning was completed, the core sections were cut into half-cores and re-boxed, and the Working halves were curated as subsamples of the whole rounds with assigned core box numbers 1000 higher than the respective Archive half (e.g. CB00355103 for Archive half CB00354103). Curation was finalized in August 2021.

Whole round X-ray radiography was carried out using a Geotek X-ray computed tomography (CT) system at the BGS Core Scanning Facility. Whole round sections that were long enough (ca. 50 cm or longer) were scanned in the liner at three angles (0, 45, and 90°) at scan rates approximating 7 min per metre. Resulting radiographic images were post-processed to optimize contrast and greyscale spread to best highlight structural elements such as fractures as well as fossils, burrows, and nodules.

Whole round sections were then scanned using a Geotek multi-sensor core logger (MSCL). Three types of analysis (gamma density GD, magnetic susceptibility MS, and natural

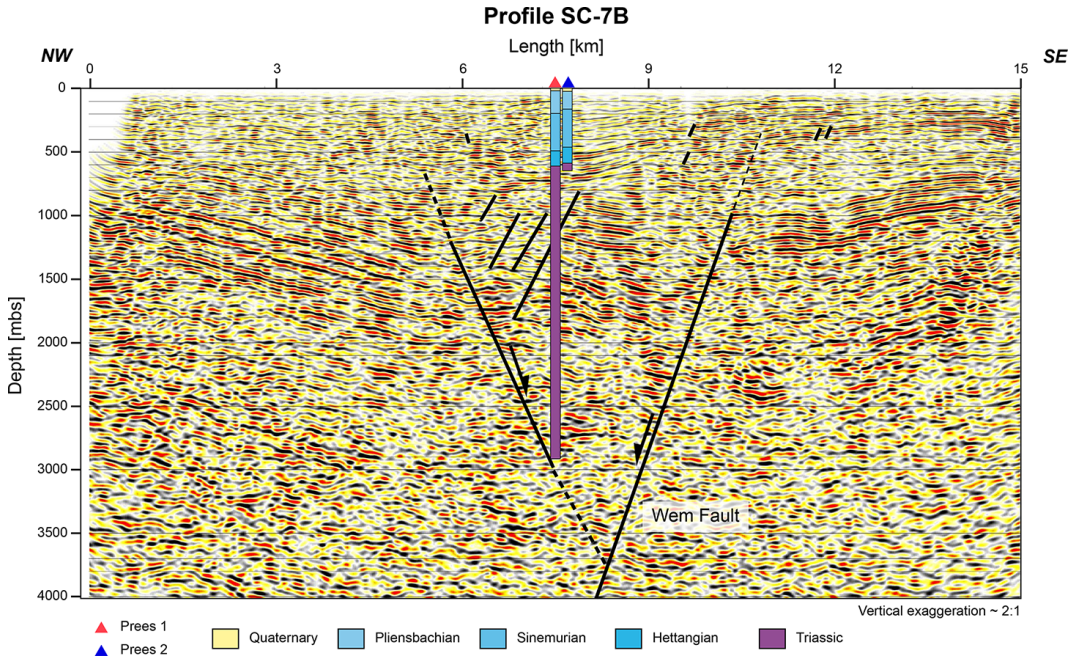

Figure 2. Migrated and depth-converted section of profile SC-7B oriented NW (left)–SE (right) (see Fig. 1 inset). The Prees 1 and Prees 2 boreholes are projected onto the seismic line. The stratigraphic units are colour-coded to match Fig. 3. Note the change in subsidence style equivalent to a depth of about 800 m at Prees, using assumed time–depth parameters, which likely corresponds to a level within the Late Triassic. Prees 1 also drilled Permian, Carboniferous, and Silurian age strata below the Triassic (not shown).

gamma-ray emission NG) were carried out at a step size of 2 cm. Data were integrated for 10 s for GD and MS and for 30 s averaging of the signal of three detectors for NG.

Core slabbing was undertaken after completion of MSCL work in batches of 28 core sections (one pallet) to avoid premature drying and development of fractures. Working and Archive halves were designated at this point, with the Archive half retaining the original core box number. After sawing of the sections, they were washed and covered with tissue to draw out saline pore liquids and avoid salt crust formation. Sections below depths of ~ 80 m required multiple rounds of rinsing and salt removal before they could be further scanned due to very high sodium chloride content.

High-resolution core photographs were taken for both the Archive and Working halves using a semi-automated layout on a scanning station at the BGS National Core Repository using a digital camera. Data were immediately uploaded to the BGS system for quality control.

Core-scanning XRF data were acquired for Archive half core sections using an Itrax core-scanning system capable of automatically processing up to five sections. Analyses were carried out in 1 cm increments with 10 s integration for each increment and peak areas were quantified using a single, preliminary model fit to the data. Image data were also acquired using this instrument.

Samples for palaeo-magnetic study were marked in 50 cm intervals on the Working half and cut using rock-sawing equipment. The sample sizes are ~ 3 × 3 × 3 cm with orientation marks scratched on the surface using a steel preparation pin (results from analysis of these samples will be presented elsewhere).

2.5 Macrofossil sampling and identification

Macrofossil sampling was undertaken on the Working half of the core, with fossils selected from inspection of bedding planes on a centimetre-by-centimetre basis in mudstone lithology. Ammonite samples dominated, and a subset of other macrofossil material specimens was also set aside. Sampling for ammonites was prioritized, and a representative selection of other macrofossil material specimens was also set aside. Each ammonite recovered was identified to the most refined taxonomic level possible, and these identifications form the basis for the biochronostratigraphic framework.

2.6 Carbon isotopes, total organic carbon, and calcium content

Bulk rock samples were crushed and ground at the BGS National Environmental Isotope Facility, generating subsamples of different size fractions. Coarse material was retained for palynological work, and fine-grained powders were split into subsamples for decarbonation and subsequent organic carbon (C_{org}) isotope analysis and subsamples for bulk geochemical analysis. Powdered and homogenized samples were de-

carbonated using a 5 % HCl solution and then neutralized through repeated dilutions with deionized water before finally being dried in a freeze drier. These samples were then analysed using an Elementar Vario ISOTOPE cube elemental analyser (EA) coupled to an Isoprime precisION isotope-ratio mass spectrometer (IRMS) with an onboard centrION continuous-flow interface system.

Carbon-isotope data are reported in delta (δ) notation per mil (‰) relative to the international reference VPDB (Vienna Pee Dee Belemnite). Carbon-isotope ratios were corrected using a two-point calibration comprising the organic analytical standard B2162 (*Spirulina* algae, Elemental Microanalysis Ltd.; −18.7 ‰, in-house value) and a laboratory working standard (BROC3, −27.6 ‰). The reference materials BROC3 and B2162 have been calibrated for $\delta^{13}C$ using IAEA-CH-6 (−10.5 ‰), USGS54 (−24.4 ‰), USGS40 (−26.4 ‰), and B2174 (urea, Elemental Microanalysis Ltd.; −36.5 ‰). BROC3 (41.3 %C and 4.9 %N) was used to calculate the carbon elemental content of samples. The within-run sample repeat average external precision (1σ) for carbon content was < 0.1 wt %, and the within-run standards' average external precision (1σ) for $\delta^{13}C$ was < 0.1 ‰.

Finely powdered bulk rock splits were analysed for bulk geochemical composition at the University of Exeter's Penryn campus using an Olympus portable XRF scanner (p-XRF) in "geochem" mode, employing 40 and 10 kV beams for 60 s each. Ca data were used to estimate carbonate content and were calibrated by determination of CO_2 emissions of a subset of 24 samples using a Sercon 20–22 gas source isotope ratio mass spectrometer at the University of Exeter's Penryn campus. The $CaCO_3$ content thus derived was then used to correct carbonate-free TOC values to true values. For simplicity, calculation of $CaCO_3$ assumes that neither siderite nor dolomite is present (which is known not to be strictly the case).

2.7 Core depth scales

The depth scales for the two shallow holes, Prees 2A and Prees 2B, are simply metres below surface (Table 1). The Prees 2C depth model for the core is more complex and is summarized in "Prees_Depth_Model.xlsx" (Supplementary Data File 1 in the Supplement). Depths for the Prees 2C core were initially assigned from information recorded in the daily drilling reports. These drillers' depths were reported as metres below floor of the drill rig (m b.r.f.) for each drilled interval (core run), which was typically 6 m. Drillers' depths were then converted into metres below surface by subtracting the measured 4.58 m offset between the rig floor and surface (Table 1) from the reported m b.r.f. value. Depth information for the top depth of individual core sections cut from the full core run was then assigned by adding the distance of the top of a core section from the top of the respective core run. The depth assignments (m b.s.) for core sections resulting from this were reported to the BGS for core curation and are thus also the curated depths for the core.

The drillers' depth assumes the top depth of each core run to be equivalent to the length of the coring string in the hole at the beginning of the core run. In the majority of cases, the extracted amount of core was nearly equivalent to the drilled interval but, depending on the effectiveness of the core catcher, deviations of a few to several tens of centimetres commonly occurred. Where material from a previously incompletely extracted core run (e.g. Core 94) was recovered (Core 95), the above assumption leads to an apparent core gap above the longer core (between cores 94 and 95) and an apparent core overlap below (between cores 95 and 96) at the curated depths.

Given that the entire length of extracted core from 50 to 650 m depth taken together deviates by only a few tens of centimetres from the drilled length, the amount of extracted core can guide depth correction. Corrected model depths have thus been constructed, and this new depth scale is denoted by m c.c.d. This is the depth scale that should normally be used for reporting any finalized data for the Prees 2C core.

A small number of assumptions was made for construction of the "metres corrected core depth" (m c.c.d.) scale. The top depths of Core runs 1 and 2 were taken to be correct as there was significant core fragmentation and core loss in Core run 1. Core run 2 recovered 5.25 m of material as opposed to a reported drilling progress of 5.20 m, so the top depth of Core run 3 of 38.92 m b.s. was shifted down by 5 cm to 38.97 m c.c.d. Core runs 4 to 6 retained their initial depth assignments as Core runs 3 to 5 all yielded significantly less material than the reported drilling progress, and the retrieved material was still heavily fractured.

With the start of Core run 6, core material was largely intact and material recovery typically within a few centimetres of the reported drilling progress. The m c.c.d. scale from this point onwards is thus anchored at an assumed correct top depth of Core run 6 where 49.92 m b.s. = 49.92 m c.c.d. From this point downwards, the top of the subsequent core run is calculated by adding the recovered length of the previous core run to the top depth of the previous core run. For example, for Core run 7, the corrected depth of 54.48 m c.c.d. derives from the top of Core run 6 of 49.92 m c.c.d., with the length of the recovered core from Core run 6 being 4.56 m (54.48 m c.c.d. = 49.92 m c.c.d. + 4.56 m). This system was followed up to (and including) Core run 98 with a top depth of 571.77 m c.c.d.

Core run 98 was characterized by significant failure of recovery due to core catcher malfunction but also additional unconstrained core loss. Further coring problems occurred in Core run 106, where core integrity and recovery were compromised over an interval of ca. 1.07 m due to failure of drilling fluid circulation and a melted liner. In order to accommodate the known core loss at these points, a new depth anchor was set at the top of Core run 106 based on the reported core top position at 603.42 m b.s. = 603.42 m c.c.d.

Core top depths for Core runs 99–105 were then calculated by subtracting the lengths of individual core runs from this anchor point. For example, the top depth of Core run 105 of 597.20 m c.c.d. derives from the top depth of Core run 106 of 603.42 m c.c.d. and the recovered length of Core run 105 of 6.22 m (597.20 m c.c.d. = 603.42 m c.c.d. − 6.22 m). This procedure results in an assumed core loss of 8 cm in Core run 98 (base Core run 98 = 573.13 m c.c.d.; top Core run 99 = 573.21 m c.c.d.), which is compatible with observations.

The remaining part of the corrected depth model is then based on the assumption that the top depth of Core run 107 is correct, i.e. 604.49 m b.s. = 604.49 m c.c.d. This assumption results in a core loss of 43 cm within Core run 106, which appears realistic given observations during coring. The TD of the core according to the length of the remaining Core runs 107 to 114 is 651.32 m c.c.d. This figure contrasts with a value of 651.45 m b.s. and suggests a residual core loss of 13 cm at the bottom of the hole.

The top depths of individual core sections were assigned in the same way as in the curated depth scale, i.e. by adding the distance between the section top and the core run top to the top depth of the core run. For example, for Core 90, the run starts at 531.46 m c.c.d. The top depth of section 1 in this run is thus also 531.46 m c.c.d. Given the length of section 90_1 being 99 cm in this core run, the top depth of section 90_2 is 532.45 m c.c.d. (531.46 m c.c.d. + 0.99 m). The section top of section 90_3 is 533.45 m c.c.d. given the length of section 90_2 of 1.00 m (533.45 m c.c.d. = 531.46 m c.c.d. + 0.99 m + 1.00 m), and so forth.

The total core loss from Core runs 6 to 114 is thus 8 + 43 + 13 cm (= 64 cm) in the range from 49.92 to 651.32 m c.c.d., yielding a core recovery of 99.89 % in this interval and an overall core recovery from 32.92 m c.c.d. to a TD of 99.68 %.

2.8 Visual core description

Visual core descriptions were carried out on the Archive half core slabs at the National Core Repository to provide sample context for interpretation of depositional environments as well as diagenetic and structural history. Each core section was described at ∼ 1 cm resolution on a proforma document into which the Archive core photograph had been inserted. Visual core descriptions were then used as a basis for construction of a summary graphic log at a scale of 3 mm = 10 m. In order to control for subjectivity in descriptions, carbonate enrichment and grey shade were adjusted using Ca count data and grey-scale data from core-scanning optical images (Sect. 2.4, 2.6).

3 Results and initial interpretation

3.1 Tectonic context

Although the Prees site is clearly in an overall extensional half-graben setting within the Cheshire Basin (Evans et al., 1993; Plant et al., 1999), the latest Triassic and Early Jurassic stratal geometries are significantly different from the bulk of the Triassic and Permian in the same location.

The main structural features in seismic profile SC-7B (Fig. 2) are a NW-dipping and SW–NE-striking major normal fault (offset about 600 m) in the south and a SE-dipping and SW–NE-striking antithetic normal fault in the north. The major normal fault is the well-known Wem Fault (see Fig. 1; Evans et al., 1993; Plant et al., 1999). An imbricate system of minor synthetic normal faults is observed between the two larger faults. The Jurassic deposits above the Permian–Triassic half-graben form a small-scale synformal basin possibly created by the downward movement of the normal fault blocks along the large antithetic and smaller synthetic normal faults, although a role for salt migration in the underlying Triassic cannot be ruled out (e.g. Hodgson et al., 1992).

As is the case for the Prees 1 drilling site, the Jurassic succession of Hettangian to Pliensbachian age appears to be tectonically undisturbed, and the borehole is located through the deepest part of the synformal structure. The thickest Jurassic succession clearly occurs at the projected location of the Prees 2 well, where it is not affected by seismically imageable faults.

Due to uncertainties in our initial time–depth conversion, the precise level at which the change in tectonic style occurs is not known; however, the Late Triassic age lithostratigraphy is complete (i.e. all formations and members of the Rhaetian age Penarth Group are present), and therefore any missing strata related to the change in subsidence style must be restricted to a level lower in the Late Triassic strata than recovered in the Prees 2C core, likely at the base of the Branscombe Mudstone (Table 2) or below. Interpretation of Line SC-7B is supported by interpretation of Line SC9-35V, which is parallel and lies ∼ 4 km to the NW. Line ESO-138 is of poor quality and does not yield any additional constraint on Jurassic stratigraphy or structure.

Line SC-4 is a SW–NE-oriented line along the axis of the basin, with Prees situated at the north-eastern end (Fig. 1). This profile confirms the general tilt of the Jurassic succession in a north-easterly direction along the axis of the basin. Line SC80-77 also approaches the Prees location at its eastern end, with the profile being oblique across the basin structure (Fig. 1). This line confirms that a reduced thickness of Jurassic strata occurs to the NW of the Prees 2 drill site and confirms the antithetic geometry of the subsidiary fault shown in Fig. 2.

https://doi.org/10.5194/sd-32-1-2023

Table 2. Lithostratigraphy of Prees 2 cores. Note: n/a – not applicable.

Group	Formation	Member	Age (epoch; age)	Depth to top of unit (m c.c.d.)	Unit thickness (m)	ICDP code 5065_1_ (Hole_Core_ Section_Depth; cm)	BGS core box no. (archive)	Unit top	Summary description of unit
n/a	n/a	n/a	Pleistocene	0.30	23.92	n/a	n/a	Thin soil 30 cm recorded	Diamictite, clay, sand and gravel
Lias	Redcar Mudstone	n/a	E. Jurassic; L. Sinemurian–E. Pliensbachian	24.22	172.75	B_1_1_72cm	CB00352862	Unconformable; the top of the formation is weathered and deformed down to ∼25.75 m.	Dark-grey massive to faintly laminated mudstone and marl; carbonate concretions throughout, including sideritic and septarian; macro and trace fossils abundant at intervals; organic enriched in the lower part, ∼ 143 to 196 m depth; intense fracturing from the unit top to ∼ 50 m.
		Prees	E. Jurassic; E.–L. Sinemurian	196.90	89.25	C_31_2_49cm	CB00354191	Downward transition of dark-grey mudstone to bioturbated fine to very fine sandstone or siltstone.	Pale-grey-buff bioturbated fine to very fine sandstone and siltstone intercalated with medium- to dark-grey mudstone; low carbonate content
		n/a	E. Jurassic; Hettangian–E. Sinemurian	286.29	306.04	C_47_1_63cm	CB00354289	Downward transition of > 1 m thick very fine sandstone or siltstone beds to the marl or mudstone with siltstone beds < 1 m)	Dark-grey massive to faintly laminated mudstone and marl; sparse carbonate concretions, including sideritic and septarian; macro and trace fossils abundant at intervals; organic enriched in organic matter below 560 m c.c.d.; lowest [∼ 5] m dark-grey planar, wavy, and crinkly laminated silty limestone and mudstone
Penarth	Lilstock	Langport	L. Triassic; Rhaetian	592.33	0.18	C_104_2_13cm	CB00354625	Sharp downward change from dark-grey, faintly laminated mudstone of the overlying formation to laminated grey mudstone	Pale olive green or grey faintly laminated limestone and laminated mudstone with scattered bioclasts and thin beds or laminae of siltstone at the base
		Cotham	L. Triassic; Rhaetian	592.51	5.52	C_104_2_31cm	CB00354625	Sharp downward change to a pale-grey/buff siltstone/limestone complex bedset	Dark-grey to pale-olive green mudstone and grey to pale-olive green siltstone and silty limestone, convolute bedding common; heterolithic wavy to lenticular bedding common; scours; the top of the unit comprises pale-grey and pale-brown silt and limestone beds, including a series of pale-grey millimetre-scale silt and limestone laminae and microbial silty limestone
	Westbury		L. Triassic; Rhaetian	598.03	7.79	C_105_1_83cm	CB00354630	Sharp downward change to massive dark-grey mudstone	Dark-grey massive to laminated (including crinkly) mudstone; occasional thin limestone, siltstone, bivalve shell, and fossiliferous (phosphatic) arenaceous beds ("bone beds"), locally cross-stratified, convoluted, or pyritic
Mercia Mudstone	Blue Anchor		L. Triassic; Rhaetian	605.82	14.52	C_107_2_34cm	CB00354642	Thin dark-grey to black arenaceous mudstone with phosphatic nodules of overlying formation resting sharply on green-grey argillaceous limestone and mudstone	Pale green to grey mudstone or siltstone with occasional beds of grey to black-brown dolomitic mudstone and yellowish-grey laminated (planar, wavy, and crinkly) brecciated dolostone with desiccation cracks; bioturbation common
	Branscombe Mudstone		L. Triassic; Rhaetian	620.34	30.98	C_109_6_00cm	CB00354658	Top of the highest consistent occurrence of medium red-brown calcareous mudstone beds	Calcareous mudstone and siltstone, red-brown with common grey-green patches, spots, and thin beds that are commonly carbonate-cemented

3.2 The Late Triassic, Early Jurassic, and Quaternary successions at Prees and regional correlation

Cores of Quaternary sand and diamict and Early Jurassic mudstone were obtained from the two shallow geotechnical holes drilled for site investigation (Prees 2A to 32.2 m b.s. and Prees 2B to 37.0 m b.s.). A core of Early Jurassic and Late Triassic mudstone was obtained from the principal hole Prees 2C from 32.92 to 651.32 m c.c.d. (see Sect. 2.7 for a discussion of the depth scales for Prees 2C). A summary of the lithostratigraphy of the Prees 2 cores is provided in Table 2 and Fig. 3, and a graphic compilation of key core-based datasets is presented in Fig. 4. A graphical summary of the downhole logging data is provided in Fig. 5. A synopsis of the overall lithological succession and a comparison to previously known lithostratigraphy are given below, working stratigraphically up from the base of the cored succession.

3.2.1 Mercia Mudstone Group, Branscombe Mudstone Formation

The Branscombe Mudstone Formation of the Mercia Mudstone Group occurs from the base of the core up to 620.34 m c.c.d. The formation comprises calcareous red-brown mudstone and siltstone, with common grey-green patches, spots, and thin beds, particularly towards the top of the unit (Figs. 3, 6, 7). There are occasional occurrences of pale-grey or brown laminated and micro-brecciated carbonate beds. Burrow mottling and trace fossils occur sporadically. The lithology is similar to that described from limited outcrops and previous cores in the region (previously referred to as the Brooks Mill Mudstone – Warrington et al., 1999; Howard et al., 2008), except that anhydrite and gypsum nodules are absent or very rare. An ephemeral lake and playa depositional environment is inferred. The age of the formation is Late Triassic (likely Rhaetian). The unit has notably low downhole resistivity values (Fig. 5) possibly related to saline pore fluids.

3.2.2 Mercia Mudstone Group, Blue Anchor Formation

The Blue Anchor Formation, 14.52 m thick, is a pale-green to grey mudstone or siltstone with occasional beds of grey to black-brown dolomitic mudstone and yellowish-grey laminated (planar, wavy, and crinkly) brecciated dolostone with desiccation cracks. Bioturbation structures and trace fossils are common (Figs. 3, 6, 7). The formation ranges up to 605.82 m c.c.d., where a sharp junction with the overlying formation is observed (Fig. 7). Elsewhere in the UK, the depositional environment of the formation has been interpreted as evaporitic lacustrine passing up into shallow marine and representing the initial regional transgression in the Rhaetian (Mayall, 1981). As for the Branscombe Mudstone, this unit of the Mercia Mudstone Group also has notably low downhole resistivity values (Fig. 5) possibly related to the presence of saline pore fluid. Three distinct cycles in a number of downhole and core log parameters (e.g. gamma, density, sonic; Figs. 4, 5) denote very well-developed ∼ 5 m scale sedimentary cycles.

3.2.3 Penarth Group, Westbury Formation

The Westbury Formation, 7.79 m thick, comprises dark-grey massive to laminated (including crinkly) mudstone with local thin limestone and siltstone beds, bivalve shell beds, and fossiliferous (phosphatic) arenaceous beds ("bone beds"); locally, cross-laminated, convoluted, or pyritic strata are observed (Figs. 3, 6, 7). The formation is relatively enriched in organic matter (up to ∼ 4 % TOC). The lithofacies at Prees is typical of the Westbury Formation across the entire UK region and was deposited in a restricted shallow marine setting (e.g. MacQuaker, 1999; Swift, 1999; Hesselbo et al., 2004). The age assignment is late Rhaetian. The relatively high gamma-ray signature reflects high clay and low carbonate content, and sonic velocities are low (Figs. 4, 5).

3.2.4 Penarth Group, Lilstock Formation

The Lilstock Formation, 5.70 m thick, comprises dark-grey to pale olive-green mudstone and grey to pale olive-green siltstone and silty limestone, with common convolute bedding. Heterolithic wavy to lenticular bedding occurs with scours. The top of the unit comprises pale-grey or pale-brown silt or limestone beds, including a series of pale-grey millimetre-scale silt or limestone laminae and possibly microbial silty limestone (Figs. 3, 6, 7). The upper 18 cm are composed of pale olive-green or grey faintly laminated limestone and laminated mudstone beds with scattered bioclasts and thin beds or laminae of siltstone at the base. This bed is identified as the "Langport Member", whilst the underlying bulk of the formation is identified as the "Cotham Member" (following the practice reported in Warrington et al., 1999).

We note that Penn (1987) and Warrington et al. (1999, their Fig. 23) indicated a thicker Langport Member in the Prees 1 well, with a top depth that corresponds to ∼ 586 m c.c.d. in Prees 2, but this seems to be based on an over-simplified interpretation of the geophysical log data, which show a distinct gamma-ray low and sonic velocity high associated at Prees with carbonate-rich and relatively organic-matter-rich shales at the base of the Lias Group (Figs. 3–5).

The depositional environment of the Cotham Member in the general area of the UK and Ireland is interpreted as marginal marine, commonly coastal in view of the extensively observed desiccation cracks and localized oolitic limestones (e.g. Hesselbo et al., 2004), although neither of these features is observed in the Prees core. The convolute bedding has been much commented upon and is interpreted as representing regionally widespread seismically induced liquefaction (Mayall, 1983; Simms, 2007; Lindström et al., 2015; Laborde-Casadaban et al., 2021). The Langport Member is understood to have been deposited in a marine environment,

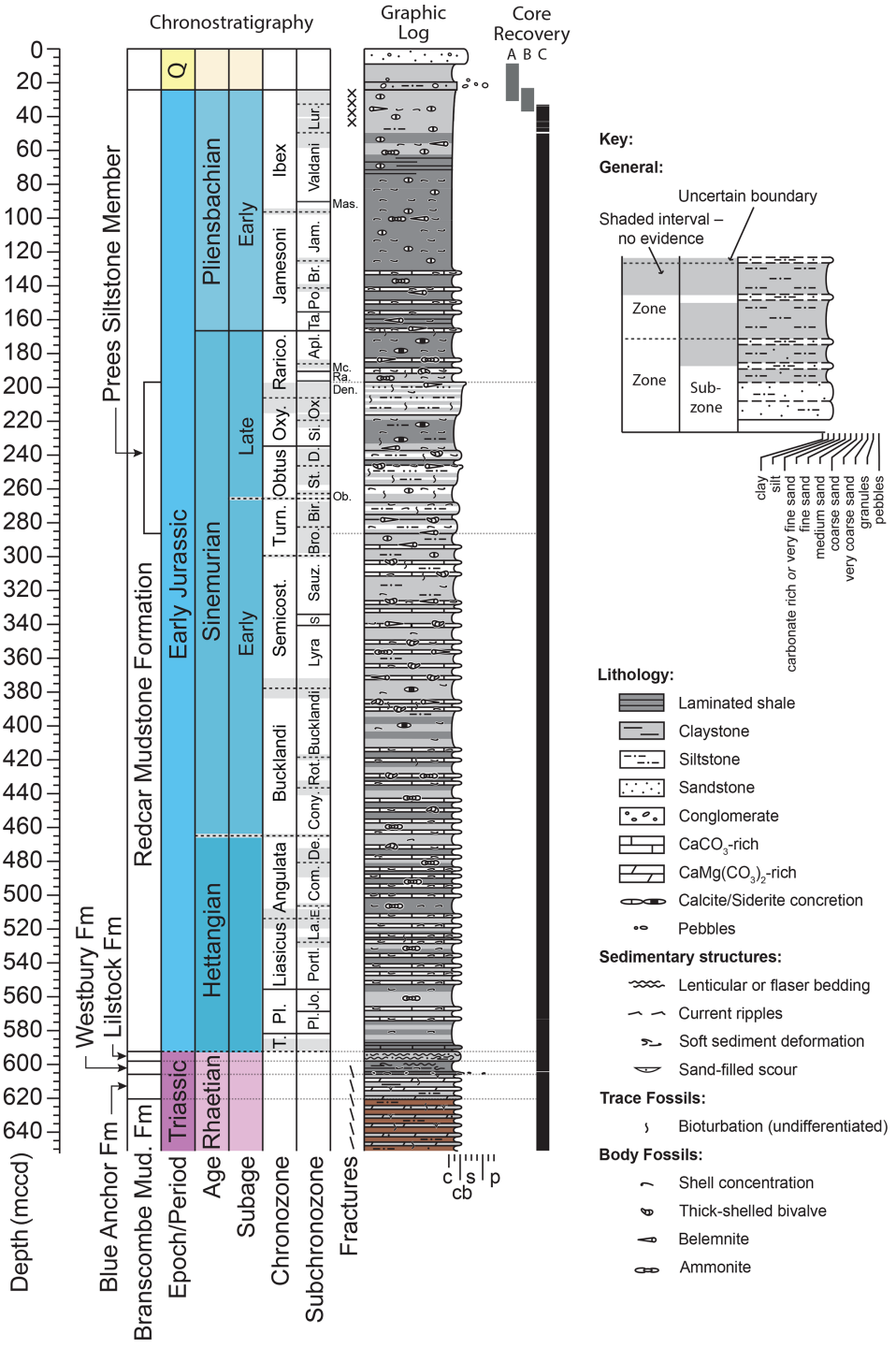

Figure 3. Summary graphic log for the recovered succession. The Branscombe Mudstone and the Blue Anchor Formation are at the top of the Mercia Mudstone Group, the Westbury Formation and the Lilstock Formation together comprise the Penarth Group, and the Redcar Mudstone here is the lowest formation of the Lias Group. Cores for the A and B site investigation holes are not yet fully documented. Abbreviations for ammonoid chronozones and subchronozones in alphabetical order – Apl.: Aplanatum; Br.: Brevispina; Bro.: Brooki; Bir.: Birchi; Com.: Complanata; Cony.: Conybeari; D.: Denotatus; Da.: Davoei; De.: Depressa; Den.: Densinodulum; E.: Extranodosa; Jam.: Jamesoni; Jo.: Johnstoni; La.: Laqueus; Lias.: Liasicus; Lur.: Luridum; Mc.: Macdonnelli; Mas.: Masseanum; Ob.: Obtusum; Ox.: Oxynotum; Pl.: Planorbis; Po.: Polymorphus; Portl.: Portlocki; Ra.: Raricostatoides; Rarico.: Raricostatum; Rot.: Rotiforme; Sauz.: Sauzei; S.: Scipionianum; Semicost.: Semicostatum; Si.: Simpsoni; St.: Stellare; T.: Tilmanni; Ta.: Taylori; Turn.: Turneri. Hybrid grain-size scale – c: clay; s: sand; p: pebble; cb: carbonate.

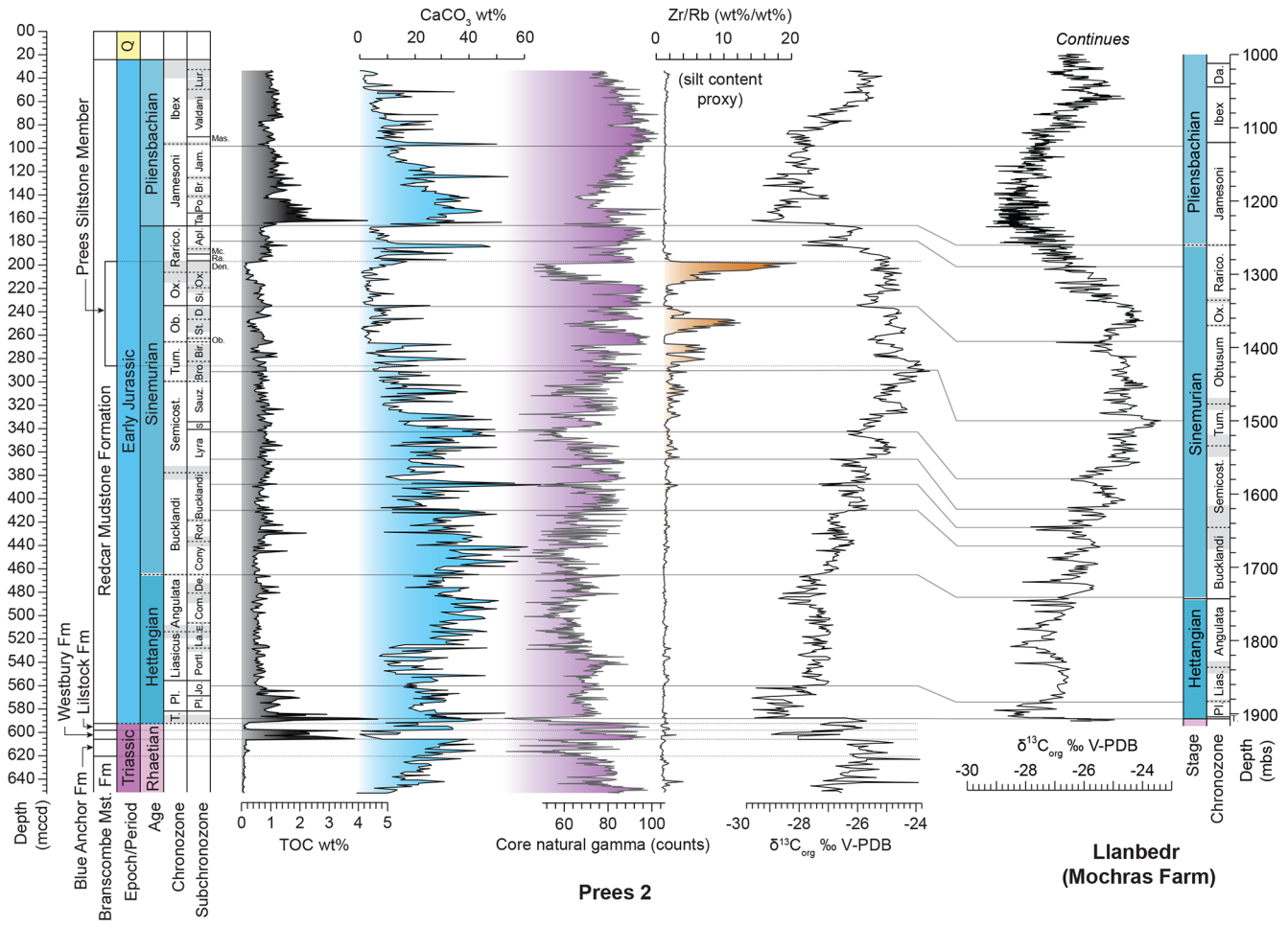

Figure 4. Summary of the succession in the Prees 2 cores and proposed correlation with the equivalent succession in the Llanbedr (Mochras Farm) borehole based on carbon-isotope stratigraphy (note the different scales used for Prees versus Mochras). Correlation lines are based on both negative and positive carbon-isotope excursions within constraints imposed by ammonite biostratigraphy. The lithological succession of the Lias Group at Prees most closely matches that of the Cleveland Basin, and thus the Redcar Mudstone Formation is adopted as the principal lithostratigraphic unit in the Cheshire Basin (Cox et al., 1999). The Prees member is defined herein. m c.c.d.: metres corrected core depth. See Fig. 3 for abbreviations of ammonoid chronozones and subchronozones. The carbon-isotope record ($\delta^{13}C_{org}$), TOC, and $CaCO_3$ data are at ~ 1 m stratigraphic resolution and are based on bulk samples. The core gamma ray is at a smoothed resolution of 20 cm. Mochras $\delta^{13}C_{org}$ from Storm et al. (2020). Data shown in this figure are tabulated in Supplementary Data Files 4–6 together with additional elements determined by p-XRF.

and in the area of the UK and Ireland it may have been deposited in a carbonate ramp to offshore shelf setting (Hesselbo et al., 2004; Jeram et al., 2021). The age assignment for both members at Prees is the latest Rhaetian (see Sect. 3.4.1).

3.2.5 Lias Group, Redcar Mudstone Formation

This formation, 568 m thick in Prees 2 and truncated below the Quaternary, comprises dark-grey massive to faintly laminated mudstone and marl. Carbonate concretions occur throughout, including sideritic and septarian varieties. Macrofossils and trace fossils are abundant at many levels, and organic matter is relatively enriched at around 590 m c.c.d. (earliest Hettangian) and 160 m c.c.d. (earliest Pliensbachian) (Figs. 3, 6, 7). The earliest Hettangian part of the formation at Prees, ~ 5 m, comprises a distinctive dark-grey, > 4 % TOC, planar, wavy, and crinkly laminated silty limestone or mudstone lithofacies, similar to some levels within the Westbury Formation at Prees. The high carbonate content in this basal unit is responsible for a markedly low downhole and core gamma-ray signature (Figs. 4, 5).

The bulk of the strata recovered in the Prees 2 cores is referred to as the Lias Group, but the formation names most appropriately used are a matter for discussion because of the previous lack of a complete record of the lower Lias Group from the Cheshire Basin (Cox et al., 1999). Names adopted could be chosen from the schemes for the south-western UK or north-eastern England. Herein we use the

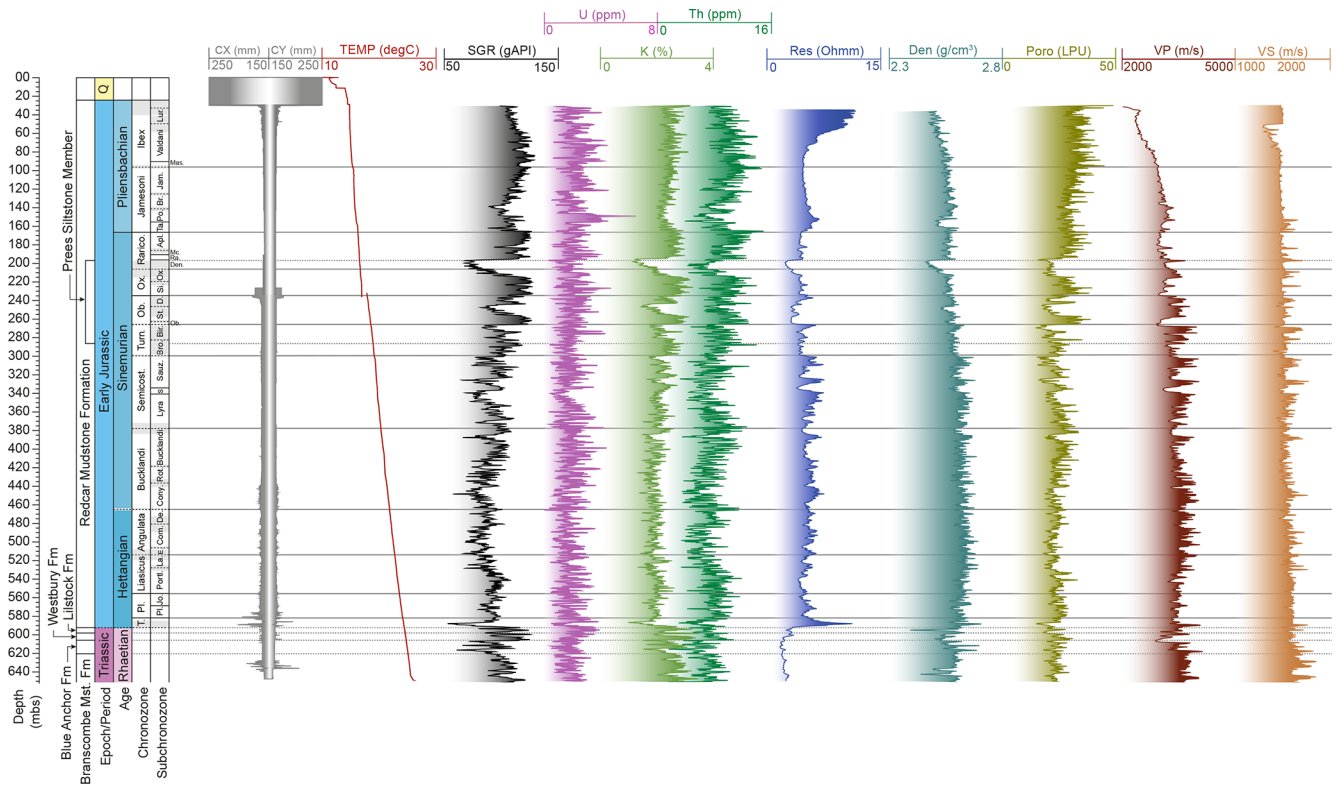

Figure 5. Summary of the downhole logging data from Prees 2C plotted against metres below the surface (m b.s.). Note that the m b.s. scale used for downhole logs generally differs only at most a few tens of centimetres from the m c.c.d. scale, except potentially at the two locations where core loss was significant, in the lowest Redcar Mudstone Formation and in the lowest Westbury Formation (see Fig. 3). From left to right: caliper (CX/CY, mm); temperature (TEMP, °C); spectral gamma ray (SGR (total), gAPI, U, ppm, K, %, Th, ppm); resistivity (Res, Ohm); density (Den, g cm^{-3}); porosity (Poro, limestone porosity units LPUs); sonic velocity (P-wave (VP), S-wave (VS), m s^{-1}).

formational name from the Cleveland Basin (Redcar Mudstone) on the basis of overall greater similarity to the Early Jurassic cropping out on the coast of north-eastern England (Yorkshire–Teesside, Cleveland Basin; Powell, 2010) compared to successions from south-western and central England and Wales (Wessex Basin, Bristol Channel Basin, and Worcester Graben; Old et al., 1987, 1991; Brandon et al., 1990; Gaunt et al., 1992; Hesselbo and Jenkyns, 1995; Warrington and Ivimey-Cook, 1995; Berridge et al., 1999).

Between 286.29 and 196.90 m c.c.d., in the Late Sinemurian interval, a distinctive unit occurs comprising pale grey-buff bioturbated fine to very fine sandstone and siltstone, intercalated with medium- to dark-grey mudstone and with a low carbonate content (generally < 10 %). This subunit is designated the "Prees Siltstone Member" herein and is correlative in time with the similarly silty and sandy Siliceous Shale Member of the Cleveland Basin Redcar Mudstone succession (e.g. Powell, 2010; Hesselbo et al., 2020b). Other similarities to the Redcar Mudstone include calcareous mudstone beds in the lower part (up to the middle of the Sinemurian, $\sim$ 340 m c.c.d.), pyritic shales around the Sinemurian–Pliensbachian boundary ($\sim$ 200–150 m c.c.d.), and nodular sideritic mudstones in the Pliensbachian ($\sim$ 100 m c.c.d. and above). The lower, more calcareous part of the recovered succession at Prees has some distinct lithological and palaeontological similarities to the Blue Lias Formation of the south-western UK but lacks the characteristic fully developed limestone beds or periodically occurring finely laminated black shale beds with high (5 %–10 %) TOC content (see for example Fig. 6d). (If Blue Lias and Charmouth Mudstone names were to be adopted instead, as might be required for a nationally or supranationally applicable scheme, then, accepting a broader lithological definition for Blue Lias, the boundary between formations would lie at $\sim$ 340 m c.c.d., and the Prees Siltsone Member could be extended down to the base of the Charmouth Mudstone thus defined.) The lithostratigraphic subdivisions of the Lias Group at Prees are all clearly evident in all the core and downhole geophysical log datasets, with gamma-ray logs being influenced strongly by both carbonate and quartz silt and sand content (Figs. 4, 5).

In line with most other lower Lias Group occurrences, the succession at Prees is interpreted as being deposited in an offshore, hemipelagic, marine setting subject to periods of basin restriction and affected by wave and distal storm processes (Hallam, 1960; Weedon, 1986; van Buchem et al.,

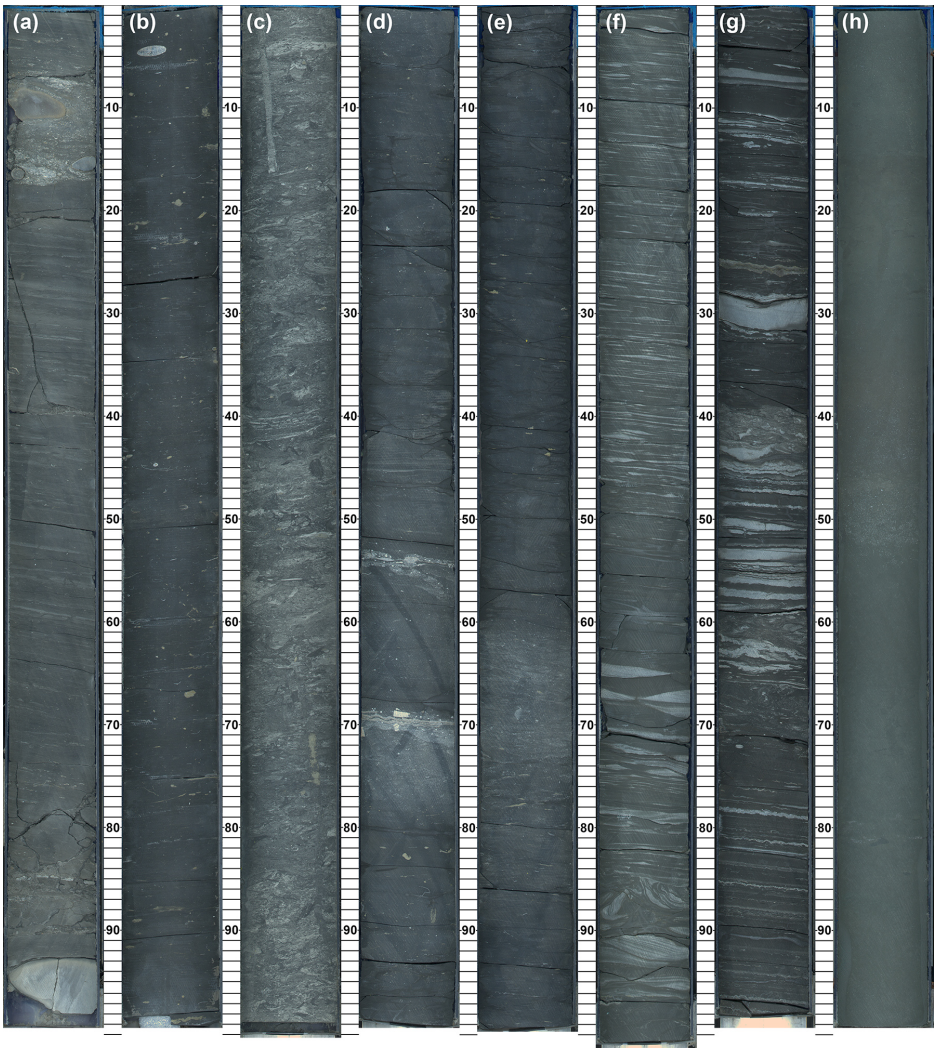

Figure 6. Typical lithofacies of Jurassic and Triassic lithological units. **(a)** Redcar Mudstone Formation, medium-grey argillaceous and siliceous mudstone with common shell debris, silty and shelly laminae and beds and red-weathering (sideritic) nodules, likely hiatus at 18 cm depth, CB00354003, 5065_1_C_2_3, 35.72–36.72 m c.c.d., Pliensbachian, ?Ibex Chronozone. **(b)** Redcar Mudstone Formation, medium- to dark-grey pyritic calcareous argillaceous mudstone, CB00354134, 5065_1_C_23_1, 146.79–147.79 m c.c.d., Pliensbachian, Jamesoni Chronozone. **(c)** Redcar Mudstone Formation, Prees Siltstone Member, pale- to medium-grey-buff bioturbated argillaceous siltstone CB00354205, 5065_1_C_33_2, 208.52–209.52 m c.c.d., Sinemurian, Oxynotum, or Raricostatum Chronozone. **(d)** Redcar Mudstone Formation, dark-grey pyritic argillaceous calcareous mudstone, CB00354454, 5065_1_C_74_2, 442.43–443.43 m c.c.d., Sinemurian, Bucklandi Chronozone. **(e)** Redcar Mudstone Formation, dark-grey and pale-grey pyritic argillaceous calcareous mudstone, CB00354531, 5065_1_C_86_4, 510.48–511.48 m c.c.d., Hettangian, Liasicus, or Angulata Chronozone. **(f)** Lilstock Formation, Cotham Member, medium–pale grey-green heterolithic mudstone with siltstone or very fine sandstone laminae and lenses, cross-laminated, with discrete levels of convolute bedding, CB00354628, 5065_1_C_104_5, 595.19–596.19 m c.c.d., Rhaetian. **(g)** Westbury Formation, dark-grey heterolithic mudstone with crinkly siltstone and carbonate laminae, with discrete levels of bioturbation structures and convolute bedding, CB00354632, 5065_1_C_105_3, 599.20–600.19 m c.c.d., Rhaetian. **(h)** Blue Anchor Formation. Grey-green calcareous argillaceous mudstone and siltstone, bioturbated, CB00354655, 5065_1_C_109_3, 617.35–618.35 m c.c.d., ?Rhaetian. All panels are Itrax optical images.

1994; Weedon et al., 2017). This setting contrasts with the Lias at Mochras, Cardigan Bay Basin, which is interpreted as having been deposited below the influence of storm processes and instead subject to contour currents and related sediment transport (Pieńkowski et al., 2021). Downhole and core gamma-ray logs provide an excellent record of metre-scale lithological cyclicity through most of the Redcar Mudstone (Figs. 4, 5).

Figure 7. Key boundaries of Jurassic and Triassic chronostratigraphic and lithostratigraphic units, marked with a red arrow head. **(a)** Sinemurian–Pliensbachian stage boundary: pale-grey bioturbated shelly calcareous mudstone rests sharply at 166.80 m c.c.d. on pale- to medium-grey shelly pyritic mudstone, carbonate-cemented in the top 9 cm; CB00354157, 5065_1_C_26_2, 166.31–167.31 m c.c.d. **(b)** Top Prees Siltstone Member, Densinodulum Subchronozone, Raricostatum Chronozone, transition of dark-grey pyritic argillaceous mudstone downward at 196.90 m c.c.d. into bioturbated fine to very fine sandstone or siltstone, CB00354191, 5065_1_C_31_2, 196.41–197.41 m c.c.d. **(c)** Base Prees Siltstone Member, Turneri Chronozone, transition downward at 286.29 m c.c.d. of pale-grey bioturbated siltstone into medium-grey argillaceous siliceous mudstone, CB00354289, 5065_1_C_47_1, 285.66–286.66 m c.c.d. **(d)** Top Lilstock Formation and Langport Member, top Cotham Member, Rhaetian; the top Langport Member has a sharp downward change from dark-grey, faintly laminated argillaceous mudstone of an overlying formation to medium-grey heterolithic laminated siltstone, limestone, and mudstone (592.33 m c.c.d.). The top Cotham Member is marked by a sharp downward change to a pale-grey or buff siltstone or limestone partly stromatolitic bedset (592.51 m c.c.d.); CB00354625, 5065_1_C_104_2, 592.20–593.19 m c.c.d. **(e)** Top Westbury Formation, Rhaetian, sharp downward change at 598.03 m c.c.d. from medium- to dark-grey convolute bedded silty mudstone to massive dark-grey argillaceous mudstone; CB00354630, 5065_1_C_105_1, 597.20–598.20 m c.c.d. **(f)** Top Blue Anchor Formation, ?Rhaetian, thin dark-grey to black arenaceous mudstone with phosphatic nodules of an overlying formation resting sharply at 605.82 m c.c.d. on green-grey argillaceous limestone and mudstone, CB00354642, 5065_1_C_107_2, 605.48–606.43 m c.c.d. **(g, h)** Top Branscombe Mudstone Formation, ?Rhaetian, top of the first consistent occurrence at 620.34 m c.c.d. of medium red-brown patches in an otherwise massive grey-green calcareous mudstone, CB00354657, 5065_1_C_109_5, 619.35–620.34 m c.c.d. and CB00354658, 5065_1_C_109_6, 620.34–621.33 m c.c.d. All panels are Itrax optical images.

3.2.6 Quaternary diamict

The lowest unit within the Quaternary succession is a red-brown diamict comprising a clay-silt matrix and abundant matrix-supported subangular to subrounded mudstone and carbonate clasts that range in colour from white through to dark grey and dark brown. The clast sizes range up to medium pebbles. The thickness of the diamict unit is estimated to be ∼4.72 m and its base is at 24.22 m b.s. However, the upper 1.38 m of the Lias Group (from 25.60 to

24.22 m b.s.) comprises a highly disturbed mudstone breccia in a mud matrix that may alternatively also be regarded as part of the Quaternary succession.

3.2.7 Quaternary clay, sand, and gravel

The upper part of the Quaternary succession comprises pebbly sand at the base (1.4 m) passing up into 6.8 m of gravelly clay and 11 m of medium sand. This unit is interpreted as part of the deltaic infill of the glacial Lake Prees (Chiverrell et al., 2021).

3.3 Fractures

3.3.1 Hydrofractures in the Lias Group

The uppermost Lias in Prees 2A and Prees 2B proved difficult to recover as fully intact cores. This is likely due to fine-scale fracture networks, particularly in the upper ∼ 7 m below the Quaternary deposits. Fractures in the strata underlying ice sheets are a widely observed phenomenon (e.g. Phillips et al., 2013; Philips and Hughes, 2014) and have been described as hydrofracture systems (Benn and Evans, 2010). At Prees, the top 1.38 m comprises dislocated angular fine pebbles and granules of mudstone in a mudstone matrix. Below this level (25.60 m b.s.), the mudstone remains in place but is highly fractured in multiple orientations down to at least 31 m b.s. Below this level the cores show common mostly bedding-parallel fracturing, but it is difficult to distinguish between natural fracture networks and those induced by drilling. The hydrofracture system at Prees is likely the result of loading by the ice mass that formed the land-terminating lobe of the Irish Sea Glacier, which was at its maximum extent during the Late Pleistocene Last Glacial Maximum (26.5 ± 1.8 ka), terminating at the glacial Lake Morville, ∼ 45 km SSE of Prees (Chiverrell et al., 2021).

3.3.2 Subvertical fractures in the Mercia Mudstone and Penarth Group

Both mineralized and unmineralized subvertical fractures occur commonly in the Triassic succession at Prees. Most cores from the Westbury Formation downwards (Core 105, 600 m c.c.d.) are affected by these fractures (Fig. 8). The fracture faces dip steeply (∼ 85°), but their compass orientation has yet to be determined. Mineralization appears to depend on host lithology in a similar manner to what is observed at Mochras (see Ullmann et al., 2022). The dense occurrence of these fractures within the Late Triassic succession suggests a relationship with the change in tectonic style at the inception of the Late Triassic to Early Jurassic sag basin. Drilling operations data (drilling fluid loss into the formation) show that these fractures remain open in the subsurface in the present day and will have significance for the sealing properties of the Mercia Mudstone Group in the Cheshire Basin and in related tectonic settings (see e.g. Al-Najdi and Worden, 2023).

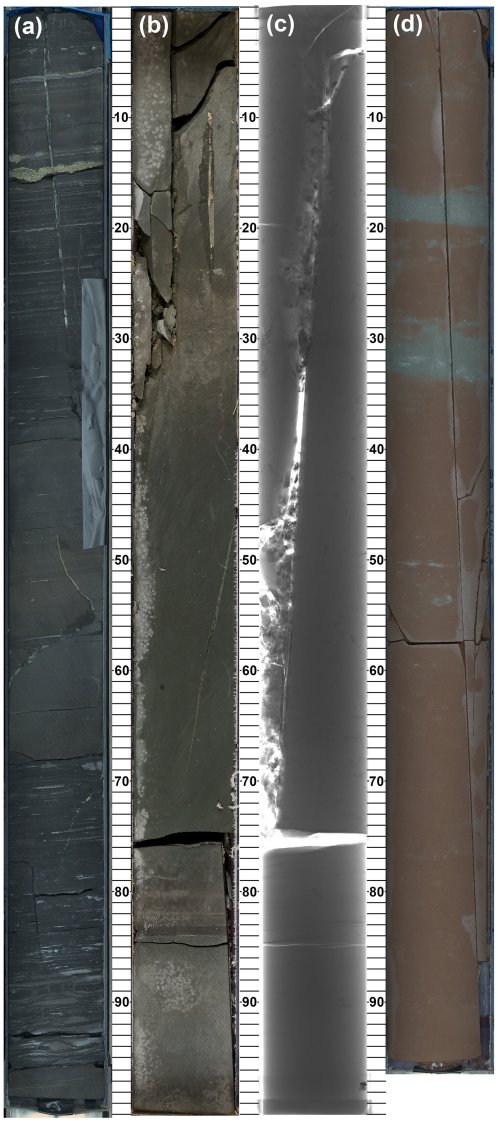

Figure 8. Subvertical fractures, Late Triassic. **(a)** Westbury Formation, subvertical mineralized fracture with millimetre-scale offset, Itrax optical image, CB00354641, 5065_1_C_107_1, 604.49–605.48 m c.c.d. **(b)** Blue Anchor Formation, subvertical mineralized fracture, core-lab photograph, CB00354644, 5065_1_C_107_4, 607.37–608.37 m c.c.d. **(c)** Blue Anchor Formation, subvertical mineralized fracture, X radiograph of the whole round, CB00354644, 5065_1_C_107_4, 607.37–608.37 m c.c.d. **(d)** Branscombe Mudstone Formation, subvertical unmineralized fracture, Itrax optical image, CB00354678, 5065_1_C_112_6, 638.23–639.20 m c.c.d.

3.4 Stratigraphic correlation and depositional history

Ammonite chronostratigraphy and carbon-isotope stratigraphy

Ammonite chronostratigraphy combined with carbon-isotope stratigraphy presently provides the principal means of regional correlation of the Jurassic strata in Prees 2 cores (Fig. 3). Chronozones can be derived from Jurassic ammonoid biozones as discussed by Page (2017). Particular emphasis is placed on identification of ammonite taxa indicative of chronozones and subchronozones and biohorizons if possible, following the biostratigraphic and chronostratigraphic scheme of Page (2003, 2009, 2010a, b) and Weedon et al. (2017, 2019), and the results are summarized here in Fig. 3 and in Supplementary Data File 2. Assignment of intervals of the core that lie between the highest and lowest markers for the chronozones and subchronozones is uncertain (i.e. there is no ammonite evidence for which zone or subzone these strata belong to), and such intervals are indicated by grey shading in the graphics.

Fossils characteristic of almost all ammonite-based chronozones and subchronozones for the cored stratigraphy are recognized at Prees. Biostratigraphic characterization is particularly good for the Hettangian and Early Sinemurian (Figs. 3–5; Supplementary Data File 2). All Late Sinemurian subchronozones are also present, but the boundaries of these subdivisions are less well defined than for the strata below, and their thicknesses are evidently quite reduced in some cases (e.g. the Raricostatoides Subchronozone of the Raricostatum Chronozone; Figs. 3–5; Supplementary Data File 2). The Early Pliensbachian ammonite-based zonation is again well defined, except in the top 35 m (Ibex Chronozone).

Carbon-isotope stratigraphy based on analysis of bulk organic matter has proven to be particularly useful for local to regional and, potentially, even global correlations to help refine those based on ammonite chronostratigraphy (e.g. Al-Suwaidi et al., 2022). Although it is broadly acknowledged that the finer details of carbon-isotope curves may be due to factors under local controls, such as mixing of different organic matter components with their individual carbon-isotopic compositions (e.g. Suan et al., 2015; Fox et al., 2022), consistent patterns in different, sometimes very distant basins are nevertheless well established. Figure 4 shows a correlation between Prees 2C, based on new data, and the basal Hettangian–Early Pliensbachian of Mochras using the carbon-isotope stratigraphy of Storm et al. (2020); all correlations shown are consistent with the ammonite biostratigraphy (see Supplementary Data File 3 for refinements to the previously published ammonite chronostratigraphy for Mochras; Page in Copestake and Johnson, 2014). No doubt further tie lines could be proposed. A noteworthy feature of the carbon-isotope curve of Prees (166.70–165.90 m c.c.d.) is the abrupt negative excursion at the Sinemurian–Pliensbachian boundary, which supports the determination of a hiatus at 166.80 m c.c.d. based on sedimentological and ichnological observations (Fig. 7). The fairly prominent negative carbon-isotope excursion in Mochras at about 1310 m in the lower part of the Raricostatum Zone may be missing at another hiatus in Prees, possibly at the top of the Prees Siltstone Member, where there is a very strongly expressed transgressive surface.

Recognition of the Triassic–Jurassic boundary away from the GSSP at Kuhjoch in Austria is currently challenging due to the very rare occurrence elsewhere of the primary marker taxon, *Psiloceras spelae* (von Hillebrandt et al., 2013). In Prees, the lowest ammonite fossil in the succession, a possible psiloceratid fragment, lies at 583.57 m c.c.d., which is 8.76 m above the lithostratigraphical base of the Lias Group (Redcar Mudstone Formation), and there are no other age-diagnostic fossils recovered yet from these basal Lias mudstones. The presence of confirmed *Psiloceras erugatum* (Phillips), however, only 0.07 m higher at 583.50 m c.c.d., represents the lowest *Psiloceras* species recorded in the UK and Irish Jurassic (Bloos and Page 2000) – placing this latter level in Prees definitely in the upper part of the basal Jurassic Tilmanni Chronozone (Page, 2010a, equivalent to the Hn2 biohorizon in Weedon et al., 2017, 2019).

Recently, Jeram et al. (2021) reviewed correlations of UK basal Jurassic successions with reference to a newly published high-resolution carbon-isotope record from Larne, Northern Ireland; these authors discuss three possible correlations based on carbon-isotope stratigraphy. Here we follow the practice of several recent authors (Korte et al., 2019; Ruhl et al., 2020) who identify a secondary negative carbon-isotope excursion lying between the "initial" and "main" carbon-isotope excursions of Hesselbo et al. (2002). In lieu of further biostratigraphic data from other fossil groups, this correlation likely places the Triassic–Jurassic boundary in Prees 2C close to the junction between the Lilstock Formation and Redcar Mudstone Formation (between 592.78 and 592.19 m c.c.d., lithostratigraphically at 592.33 m c.c.d.), but the possibility remains that the system boundary lies higher in the succession (possibly as high as ∼ 589 m c.c.d.) pending study of higher-resolution carbon-isotope datasets and palynology. We interpret the isotopically light $\delta^{13}C_{org}$ values at the top of the Cotham Member of the Lilstock Formation as representing the "initial" negative carbon-isotope excursion of Hesselbo et al. (2002). Records of lower ammonites in the UK and Irish successions, including *Neophyllites lavernockensis* Hodges, as reported from the uppermost Lilstock Formation in South Wales (Hodges, 2021), would likely be of the latest Triassic age, lying as they do below the base of the Lias and below those features of the carbon-isotope curves generated from bulk organic matter samples that signify the base of the Jurassic (see e.g. Korte et al., 2019, and references therein).

4 Summary and research prospects

The data presented here provide the stratigraphic framework and depositional context for multiple ongoing studies into Early Jurassic Earth history and Earth system processes. The succession recovered in the Prees cores spans the Late Triassic mass extinction event and its aftermath, and each ammonite chronozone and subchronozone through to the Early Pliensbachian Ibex Chronozone is represented. The recovered Lias succession is predominantly argillaceous and shows the greatest similarity to the lower Lias Group in the Cleveland Basin, which lies ~ 200 km to the NE. The prospects of determination of orbital cycles look to be very good based on clearly evident 1 m scale lithological cyclicity (Figs. 6e, 7c), which finds strong expression in both the high-resolution core-scanning data and the downhole log datasets (Figs. 4, 5). The 1 m cycles likely represent precession and form the principal building blocks for construction of an astrochronology.

A carbon-isotope curve based on bulk organic matter at ~ 1 m resolution presented here is used to correlate with the Llanbedr (Mochras Farm) borehole in the adjacent Cardigan Bay Basin. The generated carbon-isotope stratigraphy corroborates curves at comparable resolution generated from bulk organic matter and fossil wood at Mochras (Storm et al., 2020) and from bulk organic matter, wood, and macrofossil carbonate in adjacent north-western European basins (e.g. Hesselbo et al., 2020b; Ullmann et al., 2022). The Hettangian and Sinemurian stages are already notable for the parallel progressive decrease in oxygen-isotope values of benthic macrofossils whilst organic matter $\delta^{13}C_{org}$ increases, suggesting that regional seawater temperature is not directly related to global carbon burial (e.g. Hesselbo et al., 2020c). New environmental palaeo-proxy data to be generated from the core can be used to test, amongst other hypotheses, whether opening of the Hispanic oceanic corridor to the west may have driven tropical Tethyan waters further north into the north-western European basins (e.g. Ruvalcaba Baroni et al., 2018).

Appendix A: Organic matter characterization and thermal maturity in Mochras, Prees 1, and Wilkesley

Pyrolysis data were generated using a Vinci Rock-Eval 6 instrument (Behar et al., 2001) at the Department of Earth Sciences, University of Oxford, and the results are shown in Fig. A1 (see also Supplementary Data File 5).

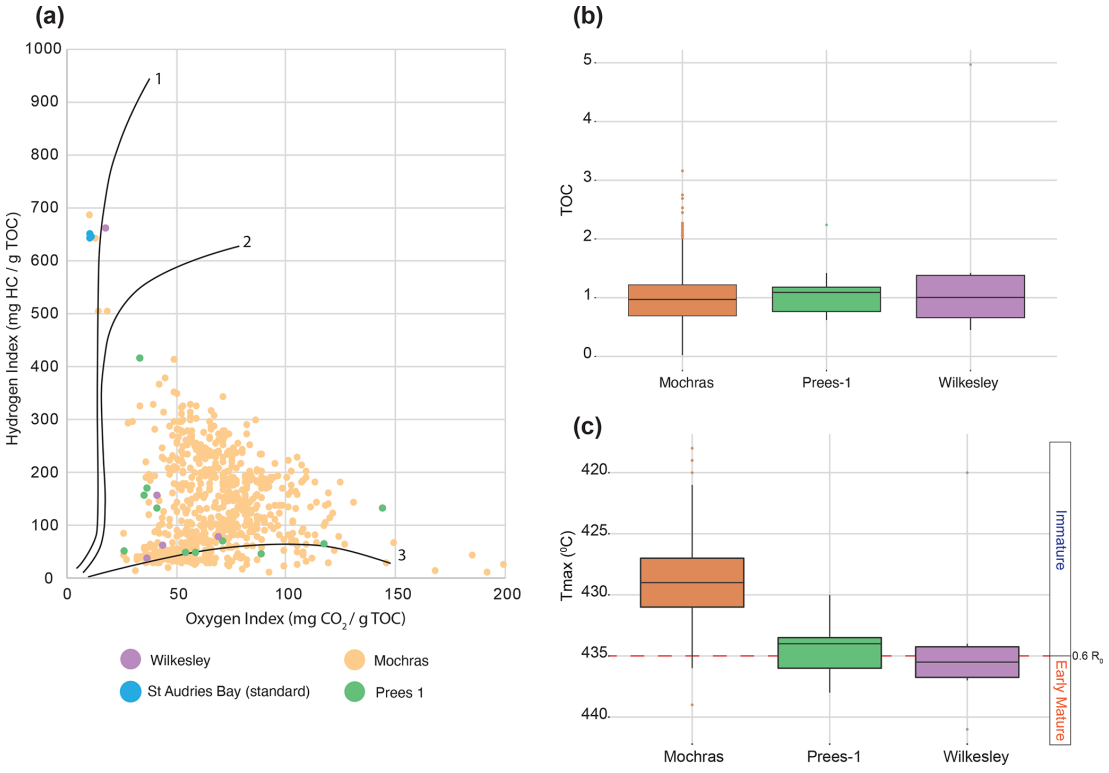

Figure A1. Rock-Eval 6 pyrolysis data. **(a)** Pyrolysis data presented in a van Krevelen diagram showing the organic matter types of the studied Prees 1 cuttings compared to Wilkesley and Mochras core samples, with outcrop samples from St Audries Bay, south-western England, used as standards. The Rock-Eval data for Prees 1 ($n = 11$) and Wilkesley ($n = 5$) indicate a Type-3 to mixed Type-2–Type-3 kerogen source (see e.g. Espitalié et al., 1977); one sample from the Wilkesley borehole plots is in the Type-1 zone. There is some uncertainty as to the representative nature of this distribution due to the small sample set. In addition, the small sample set from the Prees 1 and Wilkesley boreholes plots close to the large dataset ($n = 910$) from the Mochras borehole (Storm et al., 2020). **(b)** TOC box-and-whisker plots showing organic matter quantity. The box plots for Prees 1, Wilkesley, and Mochras have comparable ranges in TOC, with a median value close to 1 wt %. **(c)** Tmax box-and-whisker plots for thermal maturity (see Evenick, 2021, for a recent review). The range of Tmax values reported across the three wells is narrow and the differences in average Tmax relatively small, indicating practically the same to very marginally deeper burial for Prees 1 and Wilkesley compared to Mochras. The average Tmax recorded for Wilkesley just surpasses the Tmax = 435 °C mature-to-immature transition equivalent to vitrinite reflectance R_0 values approaching 0.6.

Data availability. Full core scan data (https://doi.org/10.5285/91392f09-25d4-454c-aece-56bde0dbf3ba, BGS Core Scanning Facility, 2022) will be available after 1 November 2024 via the Natural Environment Research Council (NERC) National Geoscience Data Centre (https://webapps.bgs.ac.uk/services/ngdc/accessions/index.html#, last access: 12 October 2023). Downhole logging data (https://doi.org/10.5880/ICDP.5065.001, Wonik, 2023) will be made available via the ICDP (https://www.icdp-online.org/projects/by-continent/europe/jet-uk/, last access: 12 October 2023).

The JET Operational Report is published as Hesselbo et al. (2023); full information about the operational dataset, the logging dataset, data availability and the explanatory remarks is available on the ICPD-JET project website: https://www.icdp-online.org/projects/by-continent/europe/jet-uk/ (last access: 12 October 2023).

A subset of data, additional biostratigraphic tables, and vector graphics files for Figs. 3–5 are included as the Supplement. Supplementary Data File 1 tabulates the corrected depth scale for Prees 2C. Supplementary Data File 2 summarizes the ammonite-based chronostratigraphy of the Prees 2 cores (ammonite identifications by Kevin N. Page). Supplementary Data File 3 summarizes the ammonite-based chronostratigraphy for the Hettangian to Early Pliensbachian of the Llanbedr (Mochras Farm) borehole (updated by Kevin N. Page). Supplementary Data File 4 tabulates the organic carbon-isotope ratios, TOC, and carbonate content of low-resolution samples taken at the Prees drill site; TOC and carbonate data are calculated using calibration based on portable XRF (Supplementary Data File 5) and a gas source isotope ratio mass spectrometer (Supplementary Data File 6). Supplementary Data File 5 tabulates portable XRF results for bulk rock powders of low-resolution samples taken at the Prees drill site; uncertainties stated in the table are given for the fit to the raw data and do not reflect the true reproducibility of the data. Empty fields indicate values under the detection limit. Sample SSK116001 acted as a repeat sample which was measured 70 times over the course of the data acquisition to determine the repeatability and drift of the instrument. LE stands for "light elements". Supplementary Data File 6 tabulates gas source isotope ratio mass spectrometry (GS-IRMS) data (oxygen- and carbon-isotope ratios of carbonate as well as carbonate content calculated as calcite) for a set of 24 samples covering the entire core length and reflecting a representative spread of carbonate content. Comparison of GS-IRMS data with p-XRF data was used to create a calibration curve to calculate the carbonate (and TOC) content of all low-resolution samples. Supplementary Data File 7 tabulates pyrolysis data (Rock-Eval 6) for Prees 1 well cuttings and Wilkesley borehole samples. Supplementary Data File 8 contains vector graphics files (.svg) for Figs. 3–5.

Sample availability. Samples will be available on request to the British Geological Survey National Geological Repository after 1 November 2024.

Supplement. The supplement related to this article is available online at: https://doi.org/10.5194/sd-32-1-2023-supplement.

Author contributions. All the authors contributed to the investigation. The project was conceptualized by SPH, CJB, CMB, JVB, DJC, SD, AJD, AF, LAH, CH, WK, CK, CTSL, CM, EM, RJN, KGM, JP, GP, SWP, JBR, MR, MSS, GS, NT, CVU, BvdS, TW, and WX. Additional funding was acquired by SPH, CMB, DJC, SD, HCJ, MJL, TML, CTSL, CM, RJN, JP, GP, SWP, JBR, AU, CVU, BvdS, PBW, and TW. SPH, CVU, RLS, and JBR developed and co-ordinated the project methodology. SPH and CVU created the original draft manuscript. All the authors contributed to review and editing. KH and KB were project administrators.

Competing interests. The contact author has declared that none of the authors has any competing interests.

Disclaimer. Publisher's note: Copernicus Publications remains neutral with regard to jurisdictional claims made in the text, published maps, institutional affiliations, or any other geographical representation in this paper. While Copernicus Publications makes every effort to include appropriate place names, the final responsibility lies with the authors.

Acknowledgements. We enthusiastically thank the ICDP Operations Support Group for continued help and advice over many years. The professional input of all the project contractors, Zetland Group, Zenith Energy, Marriott Drilling Group, Fox (Owmby) Ltd, Excellence Logging, and Robertson Geo, is all gratefully acknowledged. We thank the landowners, Grafton Beddoes & Sons, for access and hospitality. David J. Smith (BGS Edinburgh) provided hugely valued advice in the initial stages of this project. Staff at the BGS National Geological Repository and Core Scanning Facility, British Geological Survey, Keyworth, are warmly thanked for their long-standing support. Emma Cieslak-Jones and Connor O'Keeffe are thanked for helping with palaeontological collections and curation. Contributions to core processing at the drill site by Amy Elson and Libby Robinson are gratefully acknowledged, as is input at the original JET workshop from Hemmo Abels, Joachim Blau, Linhao Fang, Adam Robinson, Charlotte Sweeney, Christian Meister, and Ken Williford. We also thank Simon Holford and Jonathan Turner for their advice and encouragement. Daniel J. Condon, Magret Damaschke, Melanie J. Leng, and James B. Riding all publish with the approval of the Executive Director, British Geological Survey (NERC). This project would not have been possible without the sustained support of Helen Butler, Chrysten Cole, Sam Barker, Hugh McCann, and Ruth Banyard (University of Exeter). John Cope, Mike Sumbler, and Mick Oates are thanked for their discussion of the lithostratigraphy. Reviewers Paul Olsen and Sietske Batenburg provided very helpful comments on the manuscript.

Financial support. This research has been supported by the ICDP, the Natural Environment Research Council (grant no. NE/N018508/1 to Stephen P. Hesselbo, Clemens V. Ullmann, Claire M. Belcher, Timothy M. Lenton, Robert J. Newton, Crispin T. S. Little, Simon W. Poulton, and Paul B. Wignall), the German Research Foundation (grant no. 398741931 to Thomas Wonik), the Hungarian Scientific Research Fund (grant no. NN

128702 to József Pálfy), the National Science Centre, Poland (Opus 13, grant no. 2017/25/B/ST10/02235 to Gregory Pieńkowski and Alfred Uchman), and the Polish Geological Institute (grant no. 62.9012.2016.00.0 to Gregory Pieńkowski).

Review statement. This paper was edited by Thomas Wiersberg and reviewed by Sietske Batenburg and Paul Olsen.

References

AlNajdi, N. and Worden, R. H.: Porosity in mudstones and its effectiveness for sealing carbon capture and storage sites, in: Enabling Secure Subsurface Storage in Future Energy Systems, edited by: Miocic, J. M., Heinemann, N., Edlmann, K., Alcalde, J., and Schultz, R. A., Geol. Soc. Lond. Spec. Publ., 528, 339–357, https://doi.org/10.1144/SP528-2022-84, 2023.

Al-Suwaidi, A. H., Ruhl, M., Jenkyns, H. C., Damborenea, S. E., Manceñido, M. O., Condon, D. J., Angelozzi, G. N., Kamo, S. L., Storm, M., Riccardi, A. C., and Hesselbo, S. P.: New chronostratigraphic constraints on the Lower Jurassic Pliensbachian–Toarcian Boundary at Chacay Melehue (Neuquén Basin, Argentina), Sci. Rep., 12, 4975, https://doi.org/10.1038/s41598-022-07886-x, 2022.

Antell, G. S. and Saupe, E. E.: Bottom-up controls, ecological revolutions and diversification in the oceans through time, Curr. Biol., 31, R1237–R1251, 2021.

Baker, S. J., Hesselbo, S. P., Lenton, T. M., and Belcher, C. M.: Charcoal evidence that rising atmospheric oxygen terminated Early Jurassic ocean anoxia, Nat. Commun., 8, 15018, https://doi.org/10.1038/ncomms15018, 2017.

Behar, F., Beaumont, V., and Penteado, H. L. De B.: Rock-Eval 6 Technology: Performances and Developments, Oil & Gas Science and Technology – Rev. IFP, 56, 111–134, https://doi.org/10.2516/ogst:2001013, 2001.

Benn, D. and Evans, D. J. A.: Glaciers and Glaciation, 2nd edn., Routledge, London, 816 pp., https://doi.org/10.4324/9780203785010, 2010.

Berridge, N. G., Pattison, J., Samuel, M. D. A., Brandon, A., Howard, A. S., Pharaoh, T. C., and Riley, N. J.: Geology of the country around Grantham, Memoir of the British Geological Survey, Sheet 127 (England and Wales), ISBN 0118845306, 1999.

BGS Core Scanning Facility: Prees-2C Core Scanning Dataset, NERC EDS National Geoscience Data Centre [data set], https://doi.org/10.5285/91392f09-25d4-454c-aece-56bde0dbf3ba, 2022.

Bloos, G. and Page, K.: The basal Jurassic ammonite succession in the North-West European Province – review and new results, in: Advances in Jurassic Research 2000, edited by: Hall, R. L. and Smith, P. L., Proceedings of the Fifth International Symposium on the Jurassic System, Vancouver, Canada, 12–25 August 1998, GeoResearch Forum, Trans Tech Publications, Zürich, 6, 27–40, ISBN 0878498443, ISBN 9780878498444, 2000.

Brandon, A., Sumbler, M. G., and Ivimey-Cook, H. C.: A revised lithostratigraphy for the Lower and Middle Lias (Lower Jurassic) east of Nottingham, England, P. Yorks. Geol. Soc., 48, 121–141, 1990.

Capriolo, M., Mills, B. J. W, Newton, R. J., Corso J. D., Dunhill, A. M., Wignall, P. B., and Marzoli, A.: Anthropogenic-scale CO_2 degassing from the Central Atlantic Magmatic Province as a driver of the end-Triassic mass extinction, Global Planet. Change, 209, 103731, https://doi.org/10.1016/j.gloplacha.2021.103731, 2022.

Chiverrell, R. C., Thomas, G. S. P., Burke, M., Medialdea, A., Smedley, R., Clark, M. B., C., Duller, G. A. T., Fabel, D., Jenkins, G., Ou, X., Roberts, H. M., and Scourse, J.: The evolution of the terrestrial-terminating Irish Sea glacier during the last glaciation, J. Quaternary Sci., 36, 752–779, 2021.

Copestake, P.: Triassic, in: Stratigraphical Atlas of Fossil Foraminifera, edited by: Jenkins, D. G. and Murray, J. W., 2nd edn., Ellis Horwood, Chichester, 97–124, ISBN 9780853122104, 1989.

Copestake, P. and Johnson, B.: The Hettangian to Toarcian (Lower Jurassic), in: Stratigraphical Atlas of Fossil Foraminifera, 2nd edn., Ellis Horwood Ltd., Chichester, UK, edited by: Jenkins, D. G. and Murray, J. W., 129–188, ISBN 9780853122104, 1989.

Copestake, P. and Johnson, B.: Lower Jurassic Foraminifera from the Llanbedr (Mochras Farm) Borehole, North Wales, UK, Palaeontonographical Society Monograph, Publ. 641, v. 167 (part), 1–403, https://doi.org/10.1080/02693445.2013.11963952, 2014.

Cox, B. M., Sumbler, M. G., and Ivimey-Cook, H. C.: A formational framework for the Lower Jurassic of England and Wales (onshore area), British Geological Survey Research Report RR/99/01, 1–28, 1999.

Damaschke, M., Fellgett, M. W., Howe, M. P. A., and Watson, C. J.: Unlocking national treasures: The core scanning approach, in: Core Values: the Role of Core in Twenty-first Century Reservoir Characterization, edited by: Neal, A., Ashton, M., Williams, L. S., Dee, S. J., Dodd, T. J. H., and Marshall J. D., Geol. Soc. Lond. Spec. Publ., 527, https://doi.org/10.1144/SP527-2022-58, 2022.

Deconinck, J.-F., Hesselbo, S. P., and Pellenard, P.: Climatic and sea-level control of Jurassic (Pliensbachian) clay mineral sedimentation in the Cardigan Bay Basin, Llanbedr (Mochras Farm) borehole, Wales, Sedimentology, 66, 2769–2783, 2019.

Dobson, M. R. and Whittington, R. J.: The geology of Cardigan Bay, P. Geologist. Assoc., 98, 331–353, 1987.

Espitalié, J. J., Laporte, L., Madec, M., Marquis, F., Leplat, P., Paulet, J., and Boutefeu, A.: Méthode rapide de caractérisation des roches mètres, de leur potentiel pétrolier et de leur degré d'évolution, Rev. I. Fr. Pétrol. 32, 23–45, 1977.

Evans, D. J., Rees, J. G., and Holloway, S.: The Permian to Jurassic stratigraphy and structural evolution of the Cheshire Basin, J. Geol. Soc. London, 150, 857–870, 1993.

Evenick, J. C.: Examining the relationship between Tmax and vitrinite reflectance: An empirical comparison between thermal maturity indicators, J. Nat. Gas Sci. Eng., 91, 103942021, https://doi.org/10.1016/j.jngse.2021.103946, 2021.

Fox, C. P., Whiteside, J. H., Olsen, P. E., Cui, X., Summons, R. E., Idiz, E., and Grice, K.: Two-pronged kill mechanism at the end-Triassic mass extinction, Geology, 50, 448–453, 2022.

Gaunt, G. D., Fletcher, T. P., and Wood, C. J.: Geology of the country around Kingston upon Hull and Brigg, Memoir of the British Geological Survey, Sheets 80 and 89 (England and Wales), ISBN 0118843990, 1992.

Hallam, A.: A sedimentary and faunal study of the Blue Lias of Dorset and Glamorgan, Philos. T.. Roy. Soc. Lond. B243, 1–44, 1960.

Hesselbo, S. P. and Jenkyns, H. C.: A comparison of the Hettangian to Bajocian successions of Dorset and Yorkshire, in: Field Geology of the British Jurassic, edited by: Taylor, P. D., Geol. Soc. Lond. Spec. Publ., 105–150, ISBN 1897799411, 1995.

Hesselbo, S. P., Robinson, S. A., Surlyk, F., and Piasecki, S.: Terrestrial and marine extinction at the Triassic-Jurassic boundary synchronized with major carbon-cycle perturbation: a link to initiation of massive volcanism?, Geology, 30, 251–254, 2002.

Hesselbo, S. P., Robinson, S. A., and Surlyk, F.: Sea-level change and facies development across potential Triassic–Jurassic boundary horizons, south west Britain, J. Geol. Soc. London, 161, 365–379, 2004.

Hesselbo, S. P., Bjerrum, C. J., Hinnov, L. A., MacNiocaill, C., Miller, K. G., Riding, J. B., van de Schootbrugge, B., and the Mochras Revisited Science Team: Mochras borehole revisited: a new global standard for Early Jurassic earth history, Sci. Dril., 16, 81–91, https://doi.org/10.5194/sd-16-81-2013, 2013.

Hesselbo, S. P., Ogg, J. G., and Ruhl, M.: The Jurassic Period, in: Geologic Time Scale 2020, edited by: Gradstein, F. M., Ogg, J. G., Schmitz, M. D., and Ogg, G. M., Elsevier. 955–1021, ISBN 978-0-12-824360-2, 2020a.

Hesselbo, S. P., Hudson, A. J. L., Huggett, J. M., Leng, M. J., Riding, J. B., and Ullmann, C. V.: Palynological, geochemical, and mineralogical characteristics of the Early Jurassic Liasidium Event in the Cleveland Basin, Yorkshire, UK, Newsl. Stratigr., 53, 191–211, 2020b.

Hesselbo, S. P., Korte, C., Ullmann, C. V., and Ebbesen, A.: Carbon and oxygen isotope records from the southern Laurasian Seaway following the Triassic-Jurassic boundary: parallel long-term enhanced carbon burial and seawater warming. Earth-Sci. Rev., 203, 103131, https://doi.org/10.1016/j.earscirev.2020.103131, 2020c.

Hesselbo, S. P., Ullmann, C. V., Silva, R. F. L., et al.: Early Jurassic Earth System and Timescale scientific drilling project (JET) – Operational Report, International Continental Scientific Drilling Program (ICDP), https://doi.org/10.48440/ICDP.5065.001, 2023.

Hodges, P.: A new ammonite from the Penarth Group, South Wales and the base of the Jurassic System in SW Britain, Geol. Mag., 158, 1109–1114, 2021.

Hodgson, N. A., Farnsworth, J., and Fraser, A. J.: Salt-related tectonics, sedimentation and hydrocarbon plays in the Central Graben, North Sea, UKCS, in: Exploration Britain: Geological insights for the next decade, edited by: Hardman, R. F. P., Geol. Soc. Lond. Spec. Publ., 67, 31–63, 1992.

Hollaar, T. P., Baker, S. J., Hesselbo, S. P., Deconinck, J.-F., Mander, L., Ruhl, M., and Belcher, C. M.: Wildfire activity enhanced during phases of maximum orbital eccentricity and precessional forcing in the Early Jurassic, Communications Earth & Environment, 2, 247, https://doi.org/10.1038/s43247-021-00307-3, 2021.

Hollaar, T. P., Hesselbo, S. P., Deconinck, J.-F., Damaschke, M., Ullmann, C. V., Jiang, M., and Belcher, C. M.: Environmental changes during the onset of the Late Pliensbachian Event (Early Jurassic) in the Cardigan Bay Basin, Wales, Clim. Past, 19, 979–997, https://doi.org/10.5194/cp-19-979-2023, 2023.

Howard, A. S., Warrington, G., Ambrose, K., and Rees, J. G. A formational framework for the Mercia Mudstone Group (Triassic) of England and Wales, British Geological Survey Research Report, RR/08/04, 2008.

Jeram, A. J., Simms, M. J., Hesselbo S. P., and Raine, R.: Carbon isotopes, ammonites and earthquakes: Key Triassic-Jurassic boundary events in the coastal sections of south-east County Antrim, Northern Ireland, UK, P. Geologist. Assoc., 132, 702–725, 2021.

Kent, D. V., Olsen, P. E., Rasmussen, C., Lepre, C., Mundil, R., Irmis, R. B., Gehrels, G. E., Giesler, D., Geissman, J. W., and Parker, W. G.: Empirical evidence for stability of the 405-kiloyear Jupiter–Venus eccentricity cycle over hundreds of millions of years, P. Natl. Acad. Sci. USA, 115, 6153–6158, 2018.

Knoll, A. H. and Follows, M. J.: A bottom-up perspective on ecosystem change in Mesozoic oceans, P. R. Soc. B, 283, 20161755, https://doi.org/10.1098/rspb.2016.1755, 2016.

Korte, C., Ruhl, M., Pálfy, J., Ullmann, C. V., and Hesselbo, S. P.: Chemostratigraphy across the Triassic–Jurassic boundary, in: Chemostratigraphy Across Major Chronological Boundaries, edited by: Sial, A. N., Gaucher, C., Ramkumar, M., and Ferreira, V. P., John Wiley & Sons, Inc and AGU Books, Geophysical Monograph, 240, 185–210, 2019.

Laborde-Casadaban, M., Homberg, C., Schnyder, J., Borderie, S., and Raine, R.: Do soft sediment deformations in the Late Triassic and Early Jurassic of the UK record seismic activity during the break-up of Pangea?, P. Geologist. Assoc., 132, 688–701, 2021.

Lindström, S., Pedersen, G. K., van de Schootbrugge, B., Hansen, K. H., Kuhlmann, N., Thein, J., Johansson, L., Petersen, H. I., Alwmark, C., Dybkjær, K., Weibel, R., Erlström, M., Nielsen, L. H., Oschmann, W., and Tegner, C.: Intense and widespread seismicity during the end-Triassic mass extinction due to emplacement of a large igneous province, Geology, 43, 387–390, 2015.

MacQuaker, J. H. S.: Aspects of the sedimentology of the Westbury Formation, in: Fossils of the Rhaetian Penarth Group, edited by: Swift, A. and Martill, D. M., The Palaeontological Association, London, 39–48, ISBN 090170265X, 1999.

Mayall, M. J.: The late Triassic Blue Anchor Formation and the initial Rhaetian transgression in south-west Britain, Geol. Mag., 118, 377–384, 1981.

Mayall, M. J.: An earthquake origin for synsedimentary deformation in a late Triassic (Rhaetian) lagoonal sequence, southwest Britain, Geol. Mag., 120, 613–622, 1983.

Menini, A., Mattioli, E., Hesselbo, S. P., Ruhl, M., and Suan, G.: Primary versus carbonate production in the Toarcian, a case study from the Llanbedr (Mochras Farm) borehole (Wales), Geol. Soc. Lond. Spec. Publ., 514, 59–81, 2021.

Mikkelsen, P. W. and Floodpage, J. B.: The hydrocarbon potential of the Cheshire Basin, in: Petroleum Geology of the Irish Sea and Adjacent Areas, edited by: Meadows, N. S., Trueblood, S. E, Hardman, M., and Cowan, G., Geol. Soc. Lond. Spec. Publ., 124, 16–183, 1997.

Munier, T., Deconinck, J.-F., Pellenard, P., Hesselbo, S. P., Riding, J. B., Ullmann, C. V., Bougeault, C., Mercuzot, M., Santoni, A.-L., Huret, É., and Landrein, P.: Million-year-scale alternation of warm–humid and semi-arid periods as a mid-latitude climate mode in the Early Jurassic (late Sinemurian, Laurasian Seaway), Clim. Past, 17, 1547–1566, https://doi.org/10.5194/cp-17-1547-2021, 2021.

Old, R. A., Sumbler, M. G., and Ambrose, K.: Geology of the country around Warwick, Memoir of the British Geological Survey, Sheet 184 (England and Wales), ISBN 0118844016, 1987.

Old, R. A., Hamblin, R. J. O., Ambrose, K., and Warrington, G.: Geology of the country around Redditch, Memoir of the British Geological Survey, Sheet 183 (England and Wales), ISBN 0118844776, 1991.

Olsen, P. E., Laskar, J., Kent, D. V., Kinney, S. T., Reynolds, D. J., Sha, J., and Whiteside, J. H.: Mapping Solar System chaos with the Geological Orrery, P. Natl. Acad. Sci. USA, 116, 10664–10673, 2019.

Page, K. N.: The Lower Jurassic of Europe – its subdivision and correlation, in: The Jurassic of Denmark and adjacent areas, edited by: Ineson, J. and Surlyk, F., Geol. Surv. Den. Greenl., 1, 23–59, 2003.

Page, K. N.: High resolution ammonite stratigraphy of the Charmouth Mudstone Formation (Lower Jurassic: Sinemurian-Lower Pliensbachian) in south-west England (UK), Volumina Jurassica, 7, 19–29, 2009.

Page, K. N.: Stratigraphical Framework, in: Fossils from the Lower Lias of the Dorset Coast, edited by: Lord, A. R. and Davis, P. G., Palaeontological Association Field Guide to Fossils, 13, 33–53, ISBN 1444337742, 2010a.

Page, K. N.: Ammonites, in: Fossils from the Lower Lias of the Dorset Coast, edited by: Lord, A. R. and Davis, P. G., Palaeontological Association Field Guide to Fossils, 13, 169–261, ISBN 1444337742, 2010b.

Page, K. N.: From Oppel to Callomon (and beyond!): Building a high-resolution ammonite-based biochronology for the Jurassic System, Lethaia, 50, 336–355, 2017.

Penn, I. E.: Geophysical logs in the stratigraphy of Wales and adjacent offshore and onshore area, P. Geologist. Assoc., 98, 275–314, 1987.

Percival, L. M. E., Cohen, A. S., Davies, M. K., Dickson, A. J., Hesselbo, S. P., Jenkyns, H. C., Leng, M. J., Mather, T. A., Storm, M. S., and Xu, W.: Osmium-isotope evidence for two pulses of increased continental weathering linked to Early Jurassic volcanism and climate change, Geology, 44, 759–762, 2016.

Pharaoh, T. C.: Tectonic map of Britain, Ireland and adjacent areas. Sheet 1. 1 : 500 000, British Geological Survey, Keyworth, UK, ISBN XBIT1, 1996.

Phillips, E. and Hughes, L.: Hydrofracturing in response to the development of an overpressurised subglacial meltwater system during drumlin formation: an example from Anglesey, NW Wales, P. Geologist. Assoc., 125, 296–311, 2014.

Phillips, E., Everest, J., and Reeves. H.: Micromorphological evidence for subglacial multiphase sedimentation and deformation during overpressurized fluid flow associated with hydrofracturing, Boreas, 42, 257–469, 2013.

Pieńkowski, G., Uchman, A., Ninard, K., and Hesselbo, S.P.: Ichnology, sedimentology, and orbital cycles in the hemipelagic Early Jurassic Laurasian Seaway (Pliensbachian, Cardigan Bay Basin, UK), Global Planet. Change, 207, 103648, https://doi.org/10.1016/j.gloplacha.2021.103648, 2021.

Plant, J. A., Jones, D. G., and Haslam, H. W. (Eds.): The Cheshire Basin: basin evolution, fluid movement and mineral resources in a Permo-Triassic rift setting, the British Geological Survey, Keyworth, Nottingham, 263 pp., ISBN 0852723334, 1999.

Paulsen, M. and Thibault, N.: On the occurrence of rare nannoliths (calcareous nannofossils) in the Early Jurassic and their implications for the end-Triassic mass extinction, Pap. Palaeontol., 9, e1489, https://doi.org/10.1002/spp2.1489, 2023.

Poole, E. G. and Whiteman, A. J.: Geology of the country around Nantwich and Whitchurch. Memoirs of the Geological Survey of Great Britain (England and Wales), Sheet 122, HMSO, London, ISBN 0118807668, 1966.

Powell, J. H.: Jurassic sedimentation in the Cleveland Basin: a review, P. Yorks. Geol. Soc., 58, 21–72, 2010.

Remírez, M. N. and Algeo, T. J.: Carbon-cycle changes during the Toarcian (Early Jurassic) and implications for regional versus global drivers of the Toarcian oceanic anoxic event, Earth-Sci. Rev., 209, 103283, https://doi.org/10.1016/j.earscirev.2020.103283, 2020.

Riding, J. B., Fensome, R. A., Soyer-Gobillard, M.-O., and Medlin, L. K.: A review of the dinoflagellates and their evolution from fossils to modern, Journal of Marine Science and Engineering, 11, 1, https://doi.org/10.3390/jmse11010001, 2023.

Ruhl, M., Hesselbo, S. P., Hinnov, L., Jenkyns, H. C., Xu, W., Storm, M., Riding, J. B., Minisini, D., Ullmann, C. V., and Leng, M. J.: Astronomical constraints on the duration of the Early Jurassic Pliensbachian Stage and global climatic fluctuations, Earth Planet. Sc. Lett., 455, 149–165, https://doi.org/10.1016/j.epsl.2016.08.038, 2016.

Ruhl, M., Hesselbo, S. P., Al-Suwaidi, A., Jenkyns, H. C., Damborenea, S. E., Manceñido, M., Storm, M., Mather, T., and Riccardi, A.: On the onset of Central Atlantic Magmatic Province (CAMP) volcanism, environmental and carbon-cycle change at the Triassic–Jurassic transition (Neuquén Basin, Argentina), Earth-Sci. Rev., 208, 103229, https://doi.org/10.1016/j.earscirev.2020.103229, 2020.

Ruhl, M., Hesselbo, S. P., Jenkyns, H. C., Xu, W., Silva, R. L., Matthews, K. J., Mather, T. A., Mac Niocaill, C., and Riding, J. B.: Reduced plate movement controlled onset and timing of Early Jurassic (Toarcian) Karoo-Ferrar large igneous province volcanism and global environmental change, Sci. Adv., 8, eabo0866, https://doi.org/10.1126/sciadv.abo0866, 2022.

Ruvalcaba Baroni, I., Pohl, A., van Helmond, N. A., Papadomanolaki, N. M., Coe, A. L., Cohen, A. S., van de Schootbrugge, B., Donnadieu, Y., and Slomp, C. P.: Ocean circulation in the Toarcian (Early Jurassic): a key control on deoxygenation and carbon burial on the European Shelf, Paleoceanography and Paleoclimatology, 33, 994–1012, https://doi.org/10.1029/2018PA003394, 2018.

Simms, M. J.: Uniquely extensive soft-sediment deformation in the Rhaetian of the UK: evidence for earthquake or impact? Palaeogeogr. Palaeocl., 244, 407–423, 2007.

Storm, M. S., Hesselbo, S. P., Jenkyns, H. C., Ruhl, M., Ullmann, C. V., Xu, W., Leng, M. J., Riding, J. B., and Gorbanenko, O.: Orbital pacing and secular evolution of the Early Jurassic carbon cycle, P. Natl. Acad. Sci. USA, 117, 3974–3982, 2020.

Suan, G., van de Schootbrugge, B., Adatte, T., Fiebig, J., and Oschmann, W.: Calibrating the magnitude of the Toarcian carbon cycle perturbation, Paleoceanography, 30, 495–509, 2015.

Swift, A.: Stratigraphy (including biostratigraphy), in: Fossils of the Rhaetian Penarth Group, edited by: Swift, A. and Martill, D. M., The Palaeontological Association, London, 161–167, ISBN 090170265X, 1999.

Tappin, D. R., Chadwick, R. A., Jackson, A. A., Wingfield, R. T. R., and Smith, N. J. P.: Geology of Cardigan Bay and the Bristol Channel, United Kingdom Offshore Regional Report, British Geological Survey, HMSO, 107 pp., ISBN 0118845063, 1994.

Torsvik, T. and Cocks, L. R. M.: Earth History and Palaeogeography. Cambridge University Press, Cambridge, UK, 317 pp., https://doi.org/10.1017/9781316225523, 2017.

Ullmann, C. V., Szűcs, D., Jiang, M., Hudson, A. J. L., and Hesselbo, S.P.: Geochemistry of macrofossil, bulk rock, and secondary calcite in the Early Jurassic strata of the Llanbedr (Mochras Farm) drill core, Cardigan Bay Basin, Wales, UK, J. Geol. Soc. London, 179, jgs2021-018, https://doi.org/10.1144/jgs2021-018, 2022.

Van Buchem, F. S. P., McCave, I. N., and Weedon, G. P.: Orbitally induced small-scale cyclicity in a siliciclastic epicontinental setting (Lower Lias, Yorkshire, UK), in: Orbital Forcing and Cyclic Sequences, edited by: de Boer, P. L. and Smith, D. G., Int. As. Sed., 19, 345–66, 1994.

von Hillebrandt, A., Krystyn, L., Kürschner, W. M., Bonis, N. R., Ruhl, M., Richoz, S., Schobben, M. A. N., Urlichs, M., Bown, P. R., Kment, K., McRoberts, C. A., Simms, M., and Tomasovyìch, A.: The Global Stratotype Sections and Point (GSSP) for the base of the Jurassic System at Kuhjoch (Karwendel Mountains, Northern Calcareous Alps, Tyrol, Austria), Episodes, 36, 162–198, 2013.

Warrington, G.: The Penarth Group-Lias Group succession (Late Triassic-Early Jurassic) in the East Irish Sea Basin and neighbouring areas: a stratigraphical review, in: Petroleum Geology of the Irish Sea and Adjacent Areas, edited by: Meadows, N. S., Trueblood, S. E, Hardman, M., and Cowan, G., Geol. Soc. Lond. Spec. Publ., 124, 33–46, 1997.

Warrington, G. and Ivimey-Cook, H. C.: The Late Triassic and Early Jurassic of coastal sections in west Somerset and South and Mid-Glamorgan, in: Field Geology of the British Jurassic, edited by: Taylor, P. D., Geol. Soc. Lond. Spec. Publ., 9–30, ISBN 1-897799-41-1, 1995.

Warrington, G., Wilson, A. A., Jones, N. S., Young, S. R., and Haslam, H. W.: Stratigraphy and Sedimentology, in: The Cheshire Basin: Basin Evolution, Fluid Movement and Mineral Resources in a Permo-Triassic Rift Setting, edited by: Plant, J. A., Jones, D. G., and Haslam, H. W., Keyworth, British Geological Survey, 10–40, ISBN 0852723334, 1999.

Weedon, G. P.: Hemipelagic shelf sedimentation and climatic cycles: the basal Jurassic (Blue Lias) of South Britain, Earth Planet. Sc. Lett., 76, 321–35, 1986.

Weedon, G. P., Jenkyns, H. C., and Page, K. N.: Combined sea-level and climate controls on limestone formation, hiatuses and ammonite preservation in the Blue Lias Formation, South Britain (uppermost Triassic – Lower Jurassic), Geol. Mag., 155, 1117–1149, 2017.

Weedon, G. P., Page, K. N., and Jenkyns, H. C.: Cyclostratigraphy, stratigraphic gaps and the duration of the Hettangian Stage (Jurassic): insights from the Blue Lias Formation of southern Britain, Geol. Mag., 156, 1469–1509, 2019.

Wonik, T.: Downhole logging data of the ICDP Scientific Drilling Project "Early Jurassic Earth System and Time Scale (JET)", GFZ Data Services [data set], https://doi.org/10.5880/ICDP.5065.001, 2023.

Wood, A. and Woodland, A: Borehole at Mochras, West of Llanbedr, Merionethshire, Nature, 219, 1352–1354, 1968.

Woodland, A. (Ed.): The Llanbedr (Mochras Farm) Borehole. Institute of Geological Sciences, Report 71/18, 1–116, ISBN 118802135, 1971.

Xu, W., Ruhl, M., Jenkyns, H. C., Leng, M. J., Huggett, J. M., Minisini, J. M., Ullmann, C. V., Riding, J. B., Weijers, J. W. H., Storm, M. S., and Hesselbo, S. P.: Evolution of the Toarcian (Early Jurassic) carbon-cycle and global climatic controls on local sedimentary processes (Cardigan Bay Basin, UK), Earth Planet. Sc. Lett., 484, 396–411, 2018a.

Xu, W., MacNiocaill, C., Ruhl, M., Jenkyns, H. C., Riding, J. B., and Hesselbo, S. P.: Magnetostratigraphy of the Toarcian Stage (Lower Jurassic) of the Llanbedr (Mochras Farm) Borehole, Wales: basis for a global standard and implications for volcanic forcing of palaeoenvironmental change, J. Geol. Soc. London 175, 594–604, 2018b.